EUROPEAN ORGANIZATION FOR NUCLEAR RESEARCH (CERN)

LHCb-PUB-2015-025
28th September 2016

LHCb Scintillating Fibre Tracker: Test Beam Report 2015

The LHCb Scintillating Fibre Tracker Collaboration

Abstract

This document summarizes the testbeam results of scintillating fibre mats tested at the SPS at CERN in May and November of 2015. Fibre mats consisting of 5, 6, and 8 layers (with a wider pitch) were tested for their light yield, attenuation length, single hit efficiency, and position resolution. In November 2016, one 6-layer module was additionally irradiated to the LHCb-Upgrade dose profile for fibre mats next to the beam pipe. The loss in signal was measured near the mirror.

Credits

Editors, Writers, and Data Analysis

The following people contributed text, plots or other analysis for this document:

Ana Barbara Rodrigues Cavalcante
Robert Ekelhof
Laura Gavardi
Oliver Girard
Roman Greim
Guido Haefeli
Xiaoxue (Snow) Han
Christian Joram
Matthieu Kecke
Axel Kuonen
Blake Leverington[1]
Dominik Mitzel
Janine Müller
Max Neuner
Simon Nieswand
Tobias Tekampe

Shifters

Many thanks to the following people who took shifts during the May and November 2015 test beam campaigns:

Ana Barbara Rodrigues Cavalcante[5], Robert Ekelhof[3], Laura Gavardi[3], David Gerick[7], Olivier Girard[4], Roman Greim[2], Guido Haefeli[4], Xiaoxue (Snow) Han[7], Damian Iwanicki[2], Christian Joram[5], Matthieu Kecke[7], Axel Kuonen[4], Blake Leverington[7], Dominik Mitzel[7], Janine Müller[3], Max Neuner[7], Simon Nieswand[2], Tobias Tekampe[3], Mark Tobin[4], and Jacco De Vries[6]

[1]Contact Author: b.leverington@cern.ch
[2]RWTH Aachen, Sommerfeldstr. 14, D-52074 Aachen, Germany
[3]TU Dortmund, Otto-Hahn-Str. 4, D-44227 Dortmund, Germany
[4]EPFL, BSP - Cubotron, CH-1015 Lausanne, Switzerland
[5]CERN, CH-1211 Geneva 23, Switzerland
[6]Nikhef, Science Park 105, 1098 XG Amsterdam, The Netherlands
[7]Heidelberg Universitaet, Im Neuenheimer Feld 226, 69120 Heidelberg, Germany

Contents

Chapter 1

Introduction

1.1 LHCb Upgrade

The upgrade of the LHCb detector [1], which will take place during the Long Shutdown 2 (LS2), from the end of 2018 until the end of 2020, will extend significantly the physics reach of the experiment by allowing the detector to operate at a higher instantaneous luminosity of $2 \cdot 10^{32}\,\mathrm{cm}^{-2}\,\mathrm{s}^{-1}$. At the same time a triggerless 40 MHz readout will increase the efficiency for a wide range of hadronic B decay channels. Today, the LHCb main tracking system consists of an Inner Tracker, built from silicon strip sensors, and an Outer Tracker, using 5 mm straw-tubes for the particle detection. To cope with the expected high particle multiplicities after LS2 both detectors will be replaced by a highly granular, uniform, low-mass Scintillating Fibre (SciFi) Tracker. The location of the new SciFi detector within LHCb is shown in Fig. 1.1. The conceptual design of this tracking detector is described in Ref. [2].

1.2 Test Beam

In all test beam campaigns, prototype modules of the SciFi Tracker, further described below in Section 1.3.1, were placed in the secondary mixed particle beam (for details see Section 1.7) in the North Area of the SPS Facilities. For a detailed description of the setups during each test beam see Sections 2.1 and 3.1. The goal was to understand the performance of the finished scintillating fibre mats in terms of light yield, attenuation length, spatial resolution and hit efficiency. For the SciFi tracker, the hit efficiency is the parameter of greatest interest and is a product of the threshold cuts applied on the signal clusters and the light yield distribution in each channel. In order to establish that the signal clusters belong to particle tracks that are of good quality and do not belong to secondary scattered particles, additional tracking detectors with high precision are used as telescopes to provide a clean sample of tracks.

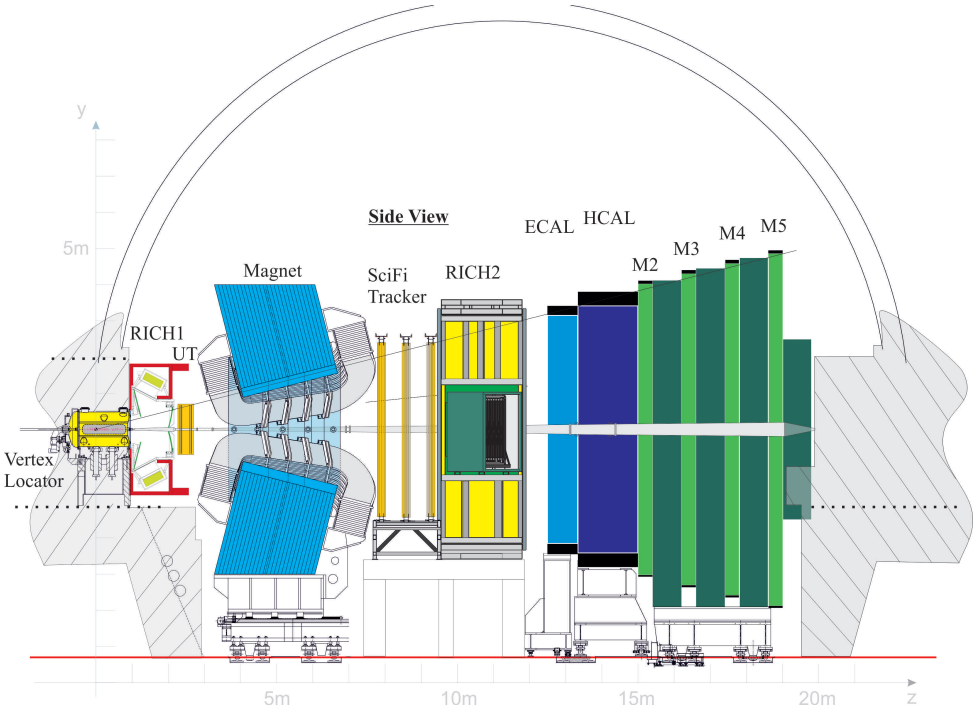

Figure 1.1: Schematic side-view of the planned upgraded LHCb detector. UT = Upstream Tracker. SciFi Tracker = Scintillating Fibre Tracker.

1.3 Detectors under test

The detectors under test (DUT) are single scintillating fibre mats, 242 cm x 13 cm, produced during development of the SciFi tracker, which have been mounted on light but stiff support structures. A module of the SciFi tracker normally has eight of these fibre mats in a 4×2 layout. Details of the production of the fibre mats and test beam modules are descibed below.

1.3.1 Module Design

The test beam modules are built from a single fibre mat sandwiched between two half-panels. The half-panels are made of 19.7 mm high Nomex honey-comb cores laminated on one side with a $200\,\mathrm{g\,m^{-2}}$ carbon-fibre reinforced polymer skin. These are the materials that will be used for the full-size module production. The two half-panels surrounding the fibre mat result in a stiff detector that can be mounted horizontally with minimal additional material in the beam line. The mat is bonded to the honeycomb with an Araldite epoxy. The module is additionally wrapped and sealed in a black foil to create a light-tight enclosure. At one end of the module, additional aluminium blocks have been added to provide for mechanical fixation and mounting of enclosures and electronics. A diagram of the module is shown in Fig. 1.2.

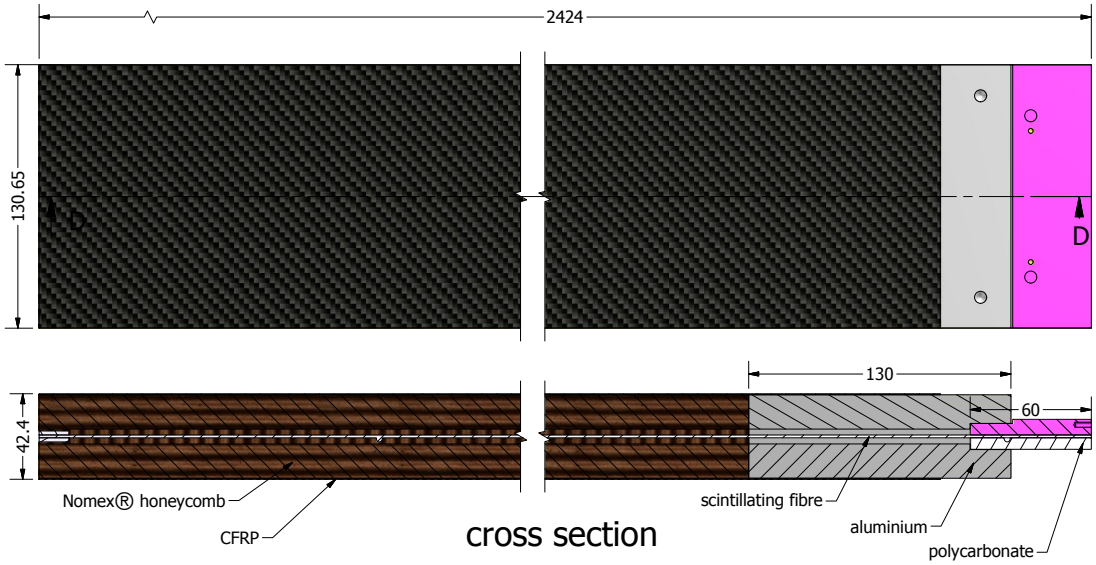

Figure 1.2: A top view and cross section of a test beam module.

1.3.2 Mat Winding

The scintillating fibre mats are the active component of the SciFi Tracker and must be assembled very precisely and with high quality. Single scintillating fibres with a 250 µm diameter are assembled into multi-layer fibre mats to produce sufficient light yield at the photo-dectectors. Each successive layer is shifted by half the horizontal pitch with respect to each other. A prototype machine was developed to produce these mats, controlling the speed and tension during winding of the fibre mats (see Fig. 1.3).

The main component of this machine is a wheel with ≈1 m diameter on which the fibres are wound. The wheel has a milled thread to guide the fibres of the first layer. The fibres of the next layers are guided by the fibres of the respective layer before. The fibre is unwound from a spool containing 12.5 km of fibre and is pre-guided by means of a small spool which moves along the width of the winding wheel. A loose spool defines the tension of the fibre and regulates the speed of the feeding spool. A two-component epoxy, Epotek 301-2, mixed with titanium dioxide (20 % w/w) is used to bond the fibres. The TiO2 reduces crosstalk between the fibres and improves the resolution. With this procedure several layers of scintillating fibres are wound. After the epoxy has cured for 24 hours or more, the fibre mat is cut perpendicular to the fibres and taken off the wheel. The pot-life of the glue was chosen such that it stays liquid enough during the winding of the five to eight layers. In addition, alignment pins made of the epoxy mixture are produced during the mat winding. Precisely milled holes in the threaded wheel surface are filled with the epoxy mixture such that they are bonded to the underside of the mat after removal.

All the fibre mats used in the test beam measurements have been produced with the prototype machine. For the serial production, a more sophisticated machine was used

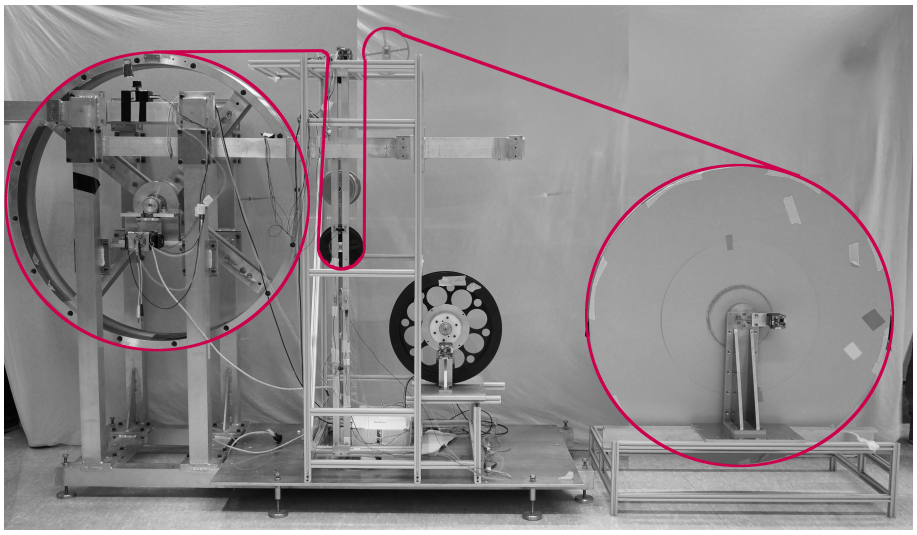

Figure 1.3: Prototype fibre winding machine. The fibre is wound from right to left and is provided by a feeding spool. A constant tension is given by a loose spool with a certain weight. A small spool gives the correct position on the winding wheel.

based on the same working principle. Further information concerning this machine or a detailed fibre mat production can be found in the Engineering Design Review (EDR) Report [3] on the CERN Document Server.

Table 1.1: The fibre mats used in the testbeam campaigns.

Name	Layers	Width / cm	X-pitch / µm	feature	Testbeam
HD1	5	7	275	no mirror, glue cast	May '15
HD2	5	13.0	275	no mirror, glue cast	May '15
Coverlay	6	13.0	280	Kapton coverlay substrate	May '15
Slayer	6	13.0	275	mirrored, glue cast	May & Nov '15
Octolayer	8	13.0	350	mirrored, foil cast	Nov '15

The scintillating fibres of type SCSF-78 (double cladded) were produced by the company Kuraray in the year 2015. A nominal fibre mat is produced with a horizontal fibre pitch of 275 µm corresponding to the milled thread in the wheel. The fibre mats HD1 and HD2 were early prototypes wound with five layers as the Perdaix prototype detector [4]. To increase the light yield such that a high hit detection efficiency is guaranteed, the SciFi baseline was set to six layers.

One protype fibre mat (Coverlay) was wound using a Kapton substrate where the grooves that aligned the first layer are produced using a coverlay technique. The resulting substrate is left bonded to the mat after winding. The success of the winding procedure using the metal wheel and some issues with the elasticity of the fibre compared to the Kapton prevented this technique from being investigated further.

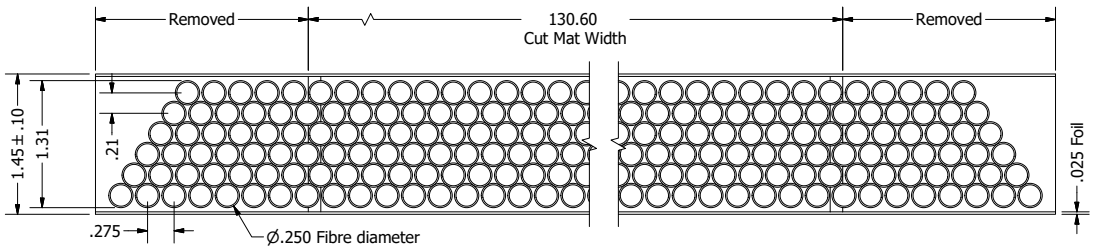

Figure 1.4: A sketch of a foil cast six layer fibre mat after winding.

Due to thick spots on the fibre, called bumps, the positioning of the fibres in the mat can be disturbed. Therefore, bumps above a certain size are removed during the winding process in a time consuming cut and re-align process. As an alternative approach fibre mats with 350 µm pitch were proposed as a possible solution. With this increased pitch the fibre can be wound more easily and less bumps have to be cut out. To get the same amount of light at the end of the fibre mat, eight instead of six layers are necessary. To study different effects of this possible modification, an eight-layer-mat with an increased pitch has been wound. The wider pitch results in only 4 % more fibre being used compared to a six layer mat, despite the eight layers. However, more epoxy is used.

Beside this, all fibre mats were wound under similar conditions. The tension during winding was 50 cN and the same amount of titanium-dioxide to dye the epoxy was used.

In addition the cross section of the mat has been analysed to check for a wrong positioning and defects in the fibre matrix. Results which exist for the mats used in the test beam can be found in Sec. A.1. Overall, these mats had few visible defects resulting from the winding. A brief description of the protective casting technique is also described in the appendix.

1.3.3 Mirrors

The mirror foils consisted of mylar foil (60 µm thickness) vacuum coated at CERN with an Al/MgF2 pair (90 nm / 20 nm thickness) coating. Epotek H301-2 epoxy glue is used to bond the mirrors. This is the same similar epoxy used during winding. Previous studies for the SciFi project have indicated that a mirror foil is supperior to other methods such as vapour deposition for improved reflectiveity [5]. Given the 13 cm width of the fibre mat, variations in the mirror quality will affect the resulting light yield and hit efficiency of the detector. The low viscocity of the epoxy while bonding the glue could also result in regions without epoxy or air bubbles, and care has been taken to minimize these effects. It is also a concern that the mirror will be in the highest region of irradiation and the transparency of the epoxy may decrease or the foil reflectivity properties could change. Studies on mirror irradiation can be found in Ref. [6].

1.4 SiPMs

Multi-channel Silicon Photo-Multipliers (SiPMs) from Hamamatsu[1] (2014 technology) are used to detect scintillation light from the fibres. The channel pitch is 250 µm and the height is 1.5 mm. A channel contains 96 pixels of a size of 57.5 µm × 62.5 µm. The detectors have 128 channels built out of two 64-channel silicon dies. Figure 1.5 shows a close-up picture of the package and pixels. A gap of 250 µm is present between the two dies. The SiPM package is mounted on a flex PCB which allows the read-out of each channel separately.

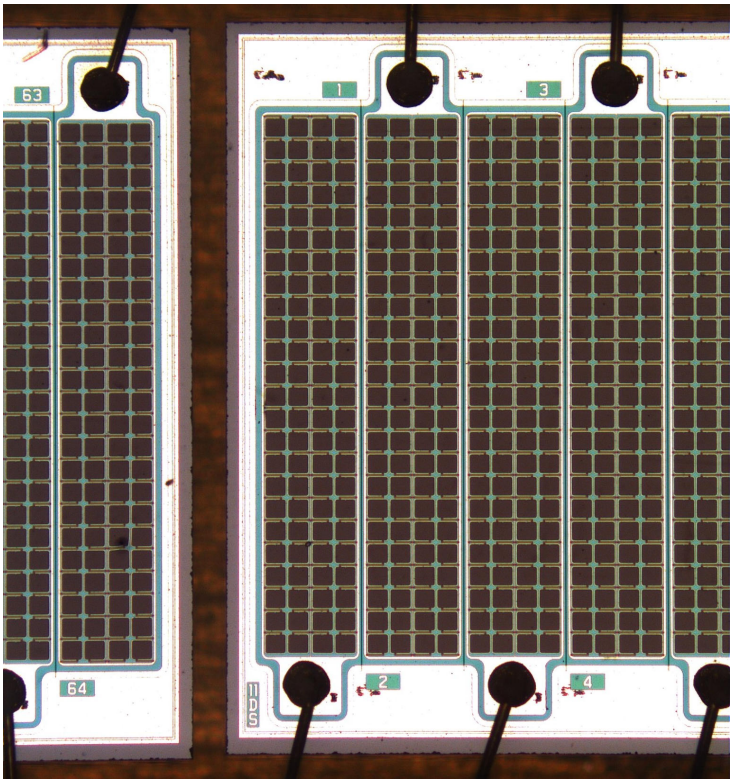

Figure 1.5: A picture taken with a microscope of the central channels of a 2014 Hamamatsu SiPM. The gap between the two dies can be seen.

The detector is characterised by the following properties:

- **Breakdown voltage** (V_{BD}) is the minimal voltage needed for an avalanche to occur. V_{BD} is given for 25 °C and is temperature dependent (54 mV K^{-1}). The operation point, or over-voltage (ΔV) is defined as $\Delta V = V_{\mathrm{bias}} - V_{\mathrm{BD}}$
- **Cross-talk** is the pixel-to-pixel cross-talk which is produced by infra-red photons created during the avalanche. The signal amplitude is one photo-electron. Opaque

[1]Hamamatsu Photonics K.K., 325-6, Sunayama-cho, Naka-ku, Hamamatsu City, Shizuoka Pref., 430-8587, Japan.

optical trenches are added to reduce the effect. Cross-talk probability is proportional to the gain. The probability of cross-talk is approximately 10 % at $\Delta V = 3.5\,\mathrm{V}$ for these devices.

- **After-pulses** are delayed avalanches produced by trapped charge in the silicon. The amplitude is variable and is in competition with the fast recovery time of the pixels. It is about 2 % at $\Delta V = 3.5\,\mathrm{V}$.
- **Photon detection efficiency** (PDE) is the ratio between the number of detected photons and the number of incident photons. The PDE peaks at 39 % at $\Delta V = 3.5\,\mathrm{V}$ at 450 nm. It is the product of three factors:
  - Quantum efficiency which is the number of electrons or holes created as photo-current divided by the number of incident photons. (nearly 100 %)
  - Fill factor(FF) which is the ratio between the active area compared to the total area. It depends on the pixel size and trench technology. (about 65 %)
  - Avalanche probability, which is the probability of the primary photo-electron to trigger the avalanche. This is dependent on the ΔV and therefore the only bias voltage (and temperature) dependent factor of the PDE.

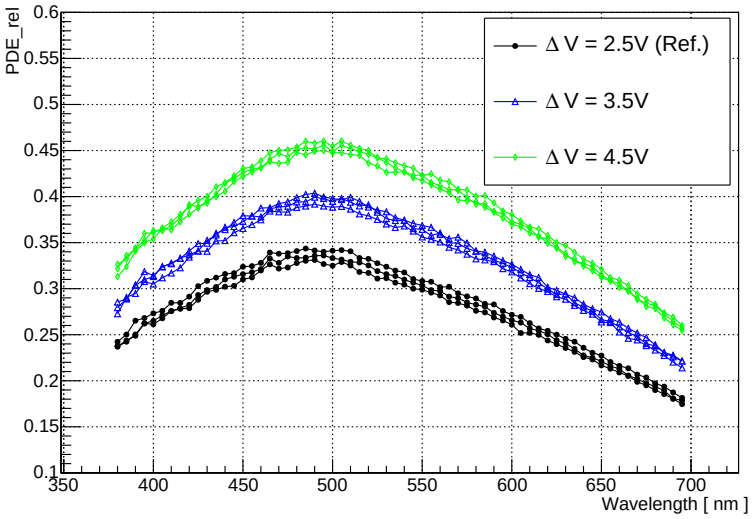

Figure 1.6: PDE for different ΔV. Peak PDE for $\Delta V = 3.5\,\mathrm{V}$ is 39 % and is situated at 490 nm.

1.5 EASIROC ASIC (a.k.a. SPIROC-A)

The EASIROC ASIC, also known as the SPIROC-A, is a 32 channel pre-amplifier ASIC with a multiplexed sample and hold stage [7]. It was designed for the SiPM of the Analogue

Hadronic Calorimeter foreseen at the International Linear Collider. The dynamical range of the channels is between 160 fC and 320 pC. Each channel splits the applied signal into two paths with a variable gain pre-amplifier and a programmable shaper. A shaping time of 200 ns was used during the testbeam measurements.

Each channel has an 8-bit DAC allowing to fine-tune the operation voltage of the detectors attached to the ASIC within 4.5 V to compensate eventual variations of the breakdown voltage of the SiPMs. The overvoltage of all SiPM array channels were calibrated and set to a default value of 3.5 V with an accuracy of 42 mV during the testbeam.

1.6 USBboard DAQ

The USBBoard is a data acquisition system (DAQ) to digitize and read out front-end boards designed for multi-channel SiPMs readout. It also provides a slow control interface to configure the front-end electronics, as well as read out on-board sensors. The system is an upgraded version of the data acquisition system previously used for the PEBS [8] experiment.

The EASIROC chip, described in Section 1.5, has a very typical structure as a multi-channel SiPM readout ASIC, which comprises a pre-amplifier, shaper and a track-and-hold block for each channel. The sampling time can be controlled by an external control signal and the sampled result for each channel is stored in an analogue buffer. All channels share one common output and are multiplex for APC conversion.

The USBBoard is designed to be a general purpose DAQ, which can read out front-end boards with different ASICs but with a similar structure as described above. Therefore, a set of readout control signals are defined and generated by the on-board FPGA, which can be interpreted as a sampling signal and channel multiplex control signals for the ASIC on the front-end board.

The main functional blocks of the USBBoard are shown in Fig. 1.7. It contains eight 12-bit ADCs, which digitize the analogue output signals from one front-end board with a 5MHz sampling. Eight independent QSPI hosts are implemented in the FPGA to provide a separate slow control interface for each front-end board. Two high voltage modules (up to 100 V/10 mA) are embedded on-board to generate two optional bias voltages for the SiPMs. There are two laser mezzanine sockets on-board, which provide all the essential signals to operate the SciFi laser mezzanines [9], so that up to 4 channels of fast-rising 5 ns-wide light pulses can be generated to calibrate the SiPMs. A plug-in USB module (QuickUSB) is used as the control and data transfer interface between the USBBoard and the PC. The maximum event rate of one single USBBoard is $\approx$1.5 kHz.

The USBBoard is an asynchronous readout system, running with a system clock of 40 MHz. A trigger signal is needed to readout the event. For each triggered event, the on-board ADC will sample the multiplexed analogue output of the front-end board channel by channel. Data of all ADCs is combined into one event data block, tagged with a 16-bit event ID and 48-bit time stamp (25 ns resolution), saved in the FIFOs and ready to be

readout by the host PC.

There are two trigger modes for the USBBoard : the Self-Trigger Mode and the External Trigger Mode. For the Self-Trigger mode, the trigger is generated by the onboard FPGA continuously at a configurable frequency, as long as the data FIFO is not full. This mode is always used for pedestal and light calibration of the detector. For the External Trigger mode, an external negative NIM level trigger signal is needed. The pulse width of the trigger signal should be 50-200 ns, in order to make sure the trigger can be registered by the DAQ correctly. Furthermore, this trigger signal should be vetoed externally by the BUSY signal sent out by the USBBoard to prevent data-taking whilst the data FIFO is full.

The interface between the USBBoard and the front-end board is defined as one Uplink, which contains the analogue output of the front-end board, one set of ASIC readout control signals, one set of SPI signals, the DAQ trigger signal fanned out via the USBBoard, biasing voltage for the SiPMs and power supply signals for the front-end board. One USBBoard comprises eight Uplinks in total and can read out up to 8 front-end boards at the same time.

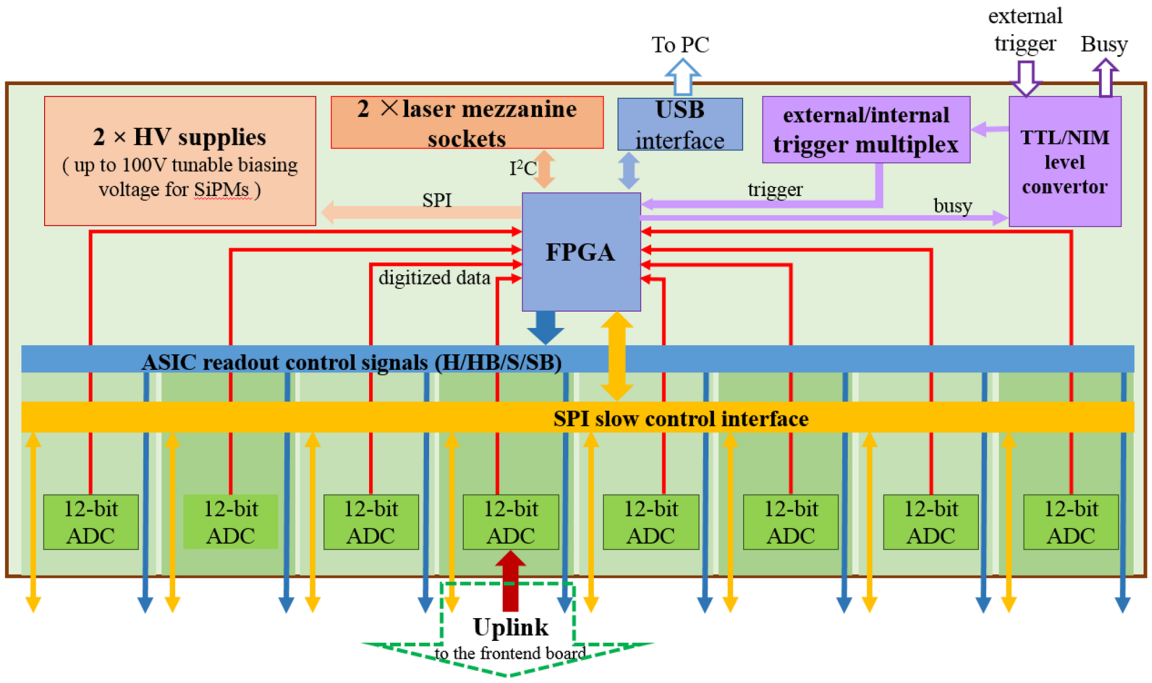

Figure 1.7: Schematics of main functional blocks and signal flow of the USBBoard

1.7 SPS beamline

The test beam campaigns took place in the LHCb area (P138) on the H8 beamline in the North Area Test Beam Facilities (EHN1) of CERN in Prévessin, France. The 450 GeV c_0^{-1}

proton beam from the SPS is incident on the T4 primary target creating a secondary beam with a mixture of pions (≈20 %), protons (≈60 %), muons (≈10 %) and some electrons with a momentum of 180 GeV $c_0{}^{-1}$. A typical spill (debunched) lasted 4.5 s and contained approximately $10 \cdot 10^6$ particles with a spill every 30 to 60 s, depending on the other facilities requiring SPS extractions.

The beam profile had a nominal width of 5 mm in the horizontal with a vertical height of 13 mm. The sharp edges are due to the collimators in the beam line, as well as the acceptance of the TimePix telescope. The profile was chosen to cover the majority of the channels of one 64-channel SiPM die. The beam profile is shown in Figure 1.8.

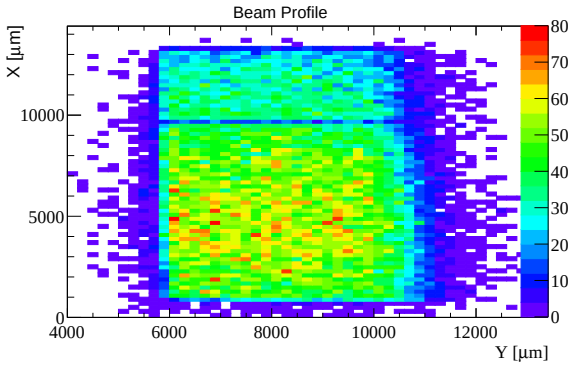

Figure 1.8: A histogram of the beam profile on one SciFi testbeam module reconstructed from the TimePix telescope tracks.

1.8 Clustering Algorithm

Charged particle tracks that pass through the fibre mat will deposit energy through ionisation in multiple scintillating fibres that are readout by one or more neighbouring SiPM channels. These signals in adjacent channels which pass a certain amplitude threshold are grouped together as clusters. From the signal information, the amplitude of the cluster in terms of the number of photo-electrons produced, and its barycentre, are calculated.

The signal amplitude is converted to units of photo-electrons by determining the gain of every SiPM channel. Slight differences across the SiPM die will produce slightly different gain and breakdown voltage values. However, the relatively constant charge from every pixel avalanche in a channel produces easily separable peaks that are observed in the ADC-distribution. The constant separation distance between photo-electron peaks is the ADC counts per photo-electron gain value for that channel. Given the need to suppress low-amplitude signals from electronics noise or thermally-induced pixel avalanches, a set of thresholds are applied to distinguish signal clusters from noise. As three thresholds are part of the 2-bit non-linear PACIFIC signal digitisation for the final SciFi Tracker electronics, it is important to simulate this threshold digitisation in the data collected with

the SPIROC electronics, which have 12-bit ADCs, and calculate the cluster barycentre as the PACIFIC would allow for. The collected cluster charge in test beam results use the full ADC information of the SPIROC front-end.

The three thresholds in the PACIFIC are defined as *low*, *middle* and *high*, as illustrated in Figure 1.9. To begin forming a cluster a channel is found that passes the middle threshold, otherwise known as the *seed* threshold. The cluster is then filled with neighbouring channels that have at least passed the low threshold, known as the *neighbour* threshold. The cluster is then checked for the total amplitude of the complete cluster. It must either have at least one channel that passes the high threshold, or one over the middle threshold plus at least one neighbour over threshold. Every channel can now be represented in terms of 3 bits (low 001, middle 010, high 100), but given that there are only four possible outcomes (000, 001, 011, 111) if low $<$ middle $<$ high , a 2-bit representation can also be used to indicate which thresholds have been passed. In 2-bits, a channel can have a value of (00, 01, 10 , or 11), or in decimal (0,1,2,3). To pass the final total cluster amplitude requirement, a cluster would require the 2-bit sum of channels as a base-10 value to be greater than or equal to 3 to be a cluster (01 + 10, 11, 01 + 11, etc.).

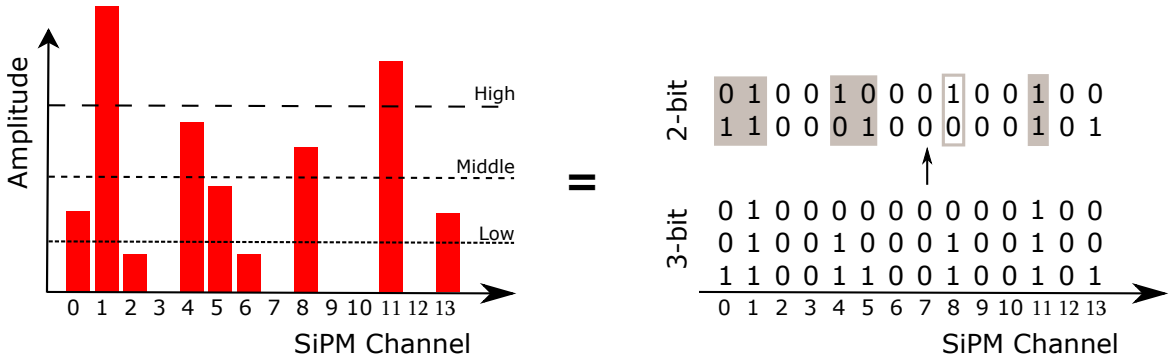

Figure 1.9: An illustration of the channel clustering using three PACIFIC-like thresholds and their 3- and 2-bit representations. The grey boxes illustrate found clusters. The open gray box fails the final sum requirement.

1.8.1 Barycentre Weighting

The barycentre of the cluster when simulating the PACIFIC response is found by weighting the channel by the mean amplitude of channels for that particular threshold pattern, as seen in the full 12-bit data. For thresholds of low = 1.5, middle = 2.5 and high = 4.5 p.e., the weights are 2, 4 and approximately 12 at the mirror, respectively. The barycentre

position of the n-th cluster is then expressed as

$$\bar{x}_n = \frac{\sum\limits_{i>Low} x_i w_i}{\sum\limits_{i>Low} w_i} \tag{1.1}$$

Table 1.2: The four possible PACIFIC bit patterns and barycentre weighting for a given channel amplitude in units of photoelectrons assuming thresholds of (1.5, 2.5, 4.5).

amp.(p.e.)	**3-bit**	**2-bit**	**base-10**	**weight**
< 1.5	000	00	0	0
1.5 – 2.5	001	01	1	2
2.5 – 4.5	011	10	2	4
> 4.5	111	11	3	12

Chapter 2

Test Beam in May 2015

2.1 Experimental setup

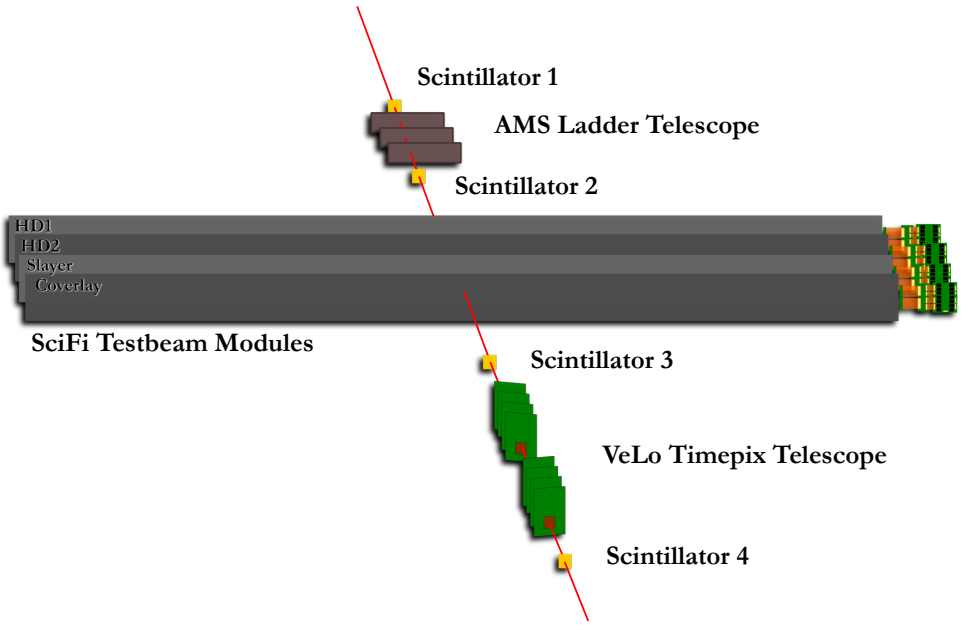

Figure 2.1: The relative detector layout with four SciFi test beam modules in H8 at the SPS in May 2015. The path of the beam is indicated by the red line.

The experimental setup of the test beam campaign in May 2015 is shown in Fig. 2.1. Four test beam modules (HD1, HD2, Slayer and Coverlay) were equipped with two SiPM arrays covering the inner 7 cm of the module. Two external telescopes, an AMS silicon ladder telescope and the VELO TimePix telescope, were used during the campaign to define reconstructed particle tracks with a resolution much better than the fibre modules, and are described further in detail below. The data acquisition triggers were formed from a coincidence of two or more scintillators. The TimePix telescope contains two small

scintillators approximately $2\,\mathrm{cm}^2$ in size. Two additional scintillators inside the AMS ladder telescope box were used to form the trigger.

The scintillation light from the fibres is detected by the silicon photo-multipliers mounted to one end of the test beam modules. The opposite sides of the fibre mats are mirrored with a film of aluminised Mylar to gain a higher light yield at the readout side. The SiPMs are read out by the SPIROC front-end boards which contain 4-8 EASIROC ASIC chips, described in Chapter 1. Each SPIROC card is connected to one of the eight uplinks of the USB-board DAQ, described in Section 1.6.

2.1.1 AMS Ladder Telescope

The AMS Ladder Telescope consists of three layers of silicon strip detectors of the Alpha Magnetic Spectrometer (AMS-02). The sensors are double sided with a pitch of 110 µm in one direction and 208 µm in the other. The single-point resolution for one of the ladders was measured to be 10 µm and 30 µm, respectively [10]. The distance between the layers is about 535 mm resulting in a track resolution between 13 and 18 µm extrapolated to the position of the first modules which can be neglected in the determination of the fibre module resolution.

The ladders are read out with USB boards which receive the same hardware trigger as the fibre modules. Therefore, the telescope provides synchronous events and tracks for all data collected during the testbeam in May 2015.

2.1.2 VELO TimePix3 Telescope

The TimePix3 telescope [11] has been developed as part of the LHCb VELO Upgrade project and consists of 8 layers of silicon hybrid pixel detectors arranged in two arms around a central DUT station. The sensitive area is formed by a $14 \times 14\,\mathrm{mm}$ matrix of $55 \times 55\,\mu\mathrm{m}$ pixels with a thickness of 300 µm that can be used to record either time or position tracking information. The eight planes are tilted to 9° in both horizontal and vertical axes to optimise the spatial resolution where the best pointing resolution of $(1.54 \pm 0.11)\,\mu\mathrm{m}$ is achieved in the centre of the telescope. At the position of the SciFi modules, about 70 cm from the telescope centre, the resolution of the track reconstruction is estimated to be about 12 µm. To record the relevant tracks, the telescope can accept an external trigger and assign time stamps with a resolution of 1 ns.

2.2 Data Analysis

Two parallel analyses have been done using reference tracks from the TimePix telescope and using tracks from the AMS telescope. The TimePix telescope was run synchronously with the fibre module readout mostly during night shifts to study important benchmark points during these data runs. The TimePix tracks could be processed quickly, and it was important to gain experience using the Timepix telescope which has greater availability

during subsequent testbeams. The data sets are typically larger for the individual points resulting in lower statistical uncertainties.

However, data taking during the day does not contain TimePix telescope tracks. The full dataset has matching AMS telescope tracks, but required some time to adapt the software after the testbeam. The readout and the analysis software are widely based on the work for a testbeam in 2009 [12] for a similar, but smaller, fibre tracker. The data sets without TimePix tracks typically have fewer events, but include more points along X and Y of the fibre modules.

2.2.1 Light Yield

The light yield is the amplitude of the signal seen in the fibre modules. In the analysis below, the amplitude is expressed in units of photoelectrons, which is a result of the photon detection efficiency of the SiPMs and the spectra of photons arriving at the detectors. The amplitudes shown are not corrected for crosstalk between pixels or saturation of the pixels, unless otherwise stated. The mean of the light yield is typically used in the analyses, rather than the most probably value (MPV) or median of the distributions. Given the variation in the path length through active scintillator in the fibre mat, the distribution deviates from the expected Landau shape seen in flat planar silicon detectors. The hit efficiency is especially sensitive to the shape of the distribution of the light yield at the lower tales due to short path lengths and fluctuations to low light yields in the scintillation mechanisms. As such, the mean was chosen, somewhat arbitrarily, to make relative comparisons of the lightyield in different conditions.

2.2.1.1 Analysis with TimePix telescope tracks

To include events with few photons, the cluster thresholds are set to 1.5 p.e. seed, 1.5 neighbour and 1.5 sum threshold, which is lower than the foreseen LHCb thresholds of (1.5, 2.5, 4.5). A higher sum threshold will bias the mean to a high mean value, if the clusters that fall below threshold are not accounted for. In the case of a missing cluster in the DUT (detector under test), a light yield of zero photons is taken into account as events are only considered when the TimePix track is correctly reconstructed in all SciFi layers. Fig. 2.2 shows the collected charge distributions of all clusters at three different horizontal positions of the module. The left one is at the mirror, the central one is in the centre of the module length and the right one is 50 cm from the SiPM. None of the values are corrected for SiPM pixel crosstalk. For comparison to the AMS ladder analysis below, only one SiPM array was illuminated by the beam, corresponding to channels 0-127 in Figure 2.6.

The mean and median light yields are given in Table 2.1. The dominant systematic uncertainty on the absolute light yield is due to a possible misalignment of the SiPM with respect to the fibre mat. It is estimated by determining the light yield for all illuminated channels separately and computing the statistical error of the mean. Some of the clusters have a large number of channels contributing, seen in Figure 2.3, which are suspected to

be a result of delta rays or crosstalk between the fibres. Since the delta electron is emitted in one direction, the position of the original particle is assumed to be at the edge in these cases. A possible modification to the clustering algorithm is to split large clusters into two 3-channel ones that are located at the edges of the large cluster. The corresponding light yield gets smaller and is given in the bottom of Table 2.1.

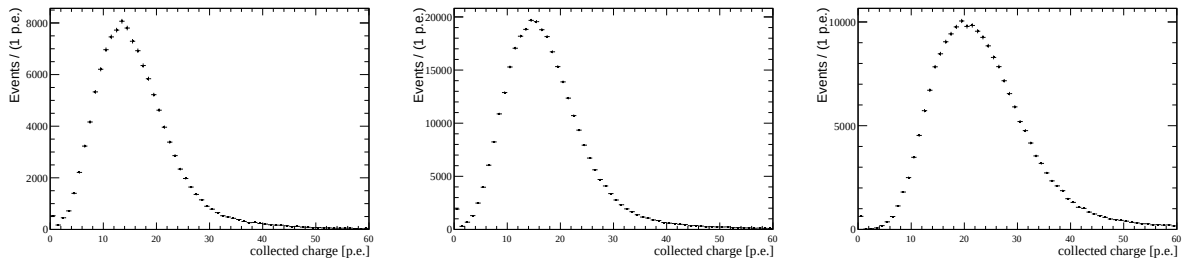

Figure 2.2: Collected charge distributions at the positions (left) at the mirror, (centre) at the centre of the module and (right) 50 cm from the SiPM. Not corrected for crosstalk.

Table 2.1: Average light yield at the mirror, at the centre of the module and 50 cm from the SiPM. Not corrected for crosstalk.

	at the mirror	centre	50 cm from SiPM
mean light yield [p.e.]	16.31 ± 0.38	17.52 ± 0.41	23.93 ± 0.54
median light yield [p.e.]	15.00 ± 0.34	16.30 ± 0.37	22.29 ± 0.50
		split large Clusters	
mean light yield [p.e.]	16.04 ± 0.37	17.29 ± 0.40	23.52 ± 0.53
median light yield [p.e.]	14.98 ± 0.34	16.29 ± 0.37	22.29 ± 0.50

The dependence of the performance on an incident angle of the beam relative to the module is investigated by tilting the module away from the beam in steps of 10 °. Table 2.2 shows the average light yield and median as a function of an incident angle at the mirror. The light yield for 50 cm from the SiPM can be seen in Table A.5 in the Appendix.

2.2.1.2 Cluster size

The cluster size here is determined for clustering thresholds (1.5, 2.5, 4.5) matching tracks to the TimePix telescope. The cluster size found for the 6-layer module at 0 degrees was found to have a mean of 2.2 with some cluster sizes extending beyond four, which is larger than what is expected from geometrical path of the primary track in the fibre. The source of these large clusters is from two possible reasons. Firstly, there is likely some crosstalk between the fibres, despite the titanium dioxide mixed into the glue of the fibre mat. It could be possible that the layer is too thin to block 100% of the light that is

Table 2.2: Average light yield at the mirror as a function of an incident angle between the beam and the module. Not corrected for crosstalk.

	0 °	10 °	20 °
mean light yield [p.e.]	16.31 ± 0.38	17.58 ± 0.39	19.08 ± 0.07
median light yield [p.e.]	15.00 ± 0.34	16.26 ± 0.35	17.73 ± 0.06
	split large Clusters		
mean light yield [p.e.]	16.04 ± 0.37	17.25 ± 0.37	18.52 ± 0.06
median light yield [p.e.]	14.98 ± 0.34	16.74 ± 0.09	17.62 ± 0.06

not captured through total internal reflection. There is also the possibility of secondaries being produced in the mat or delta electrons. The cluster size increases with the angle, as expected, with a mean size of 2.4 and 3.0 for 10 and 20 degrees, respectively. The data are shown in Figure 2.3. A positive correlation (0.6 – 0.7) between cluster size and charge is seen Figure 2.4 for the three angles analysed. Fits to the mean cluster width as a function of cluster charge with a straight line are shown in Figure 2.5. The slope of the fits appear to be independent of the beam angle, with the constant value increasing with angle. However, the data diverges from the fit significantly below 10 p.e..

2.2.1.3 Light yield Analysis with AMS ladder tracks

For the determination of the light yield only events with clean AMS telescope tracks are used, i.e. events with exactly one cluster in each of the three telescope layers in both x and y direction. In addition, events with more than one cluster are omitted. For the neighbour, seed and sum threshold, 1.5 pixels are used.

By looking at the mean cluster amplitude in Fig. 2.6 one finds a dependence on the channel number for each of the two SiPM arrays used to read out the module. This was found to stem from misalignments of the arrays. Various parameter scans were performed during the test beam campaign. In order to minimize the convolution of this slope with the actual physical parameters of the mat, it is required to use the same fibre region for each scan. Given the narrow beam size and the accuracy of the mat positioning in the beam, this can only be achieved to a certain extent. Two regions with negligible light yield slope and enough statistics could be identified for the scans: section A for horizontal scans, and section B for overvoltage and angle scans.

Fig. 2.7 shows the light yield as a function of the overvoltage provided to the arrays for two distances to the readout side: 250 cm (point A) and 50 cm (point C). Two curves are shown for each of these point. One corresponding to the raw cluster amplitude, i.e. the number of fired pixels, and the other corresponding to the cluster amplitude, corrected for saturation and crosstalk effects. The correction is done for every hit belonging to a cluster individually according to the formula [12].

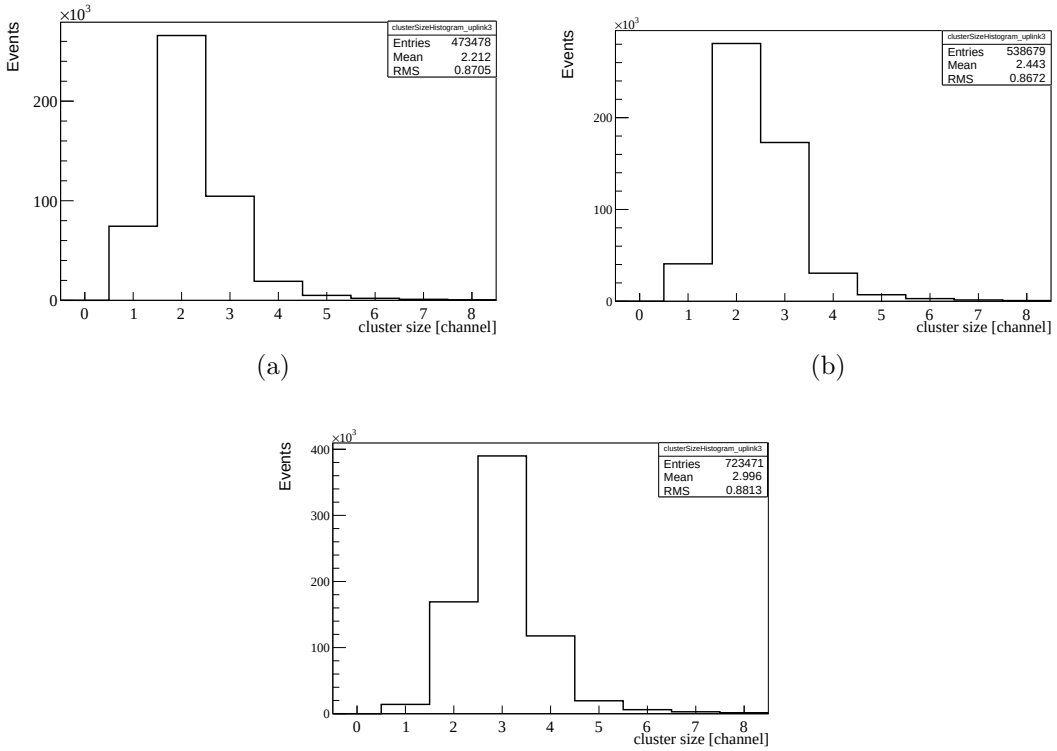

Figure 2.3: The cluster size for tracks near the mirror at a module rotation of (a) 0 , (b) 10, and (c) 20 degrees with respect to the beam.

$$n_{\text{p.e.}}^{\text{hit}} = \frac{\log\left(1 - \frac{n_{\text{pix}}^{\text{hit}}}{n_{\text{pix}}^{\text{SiPM}}}\right)}{\log\left(1 - \frac{1}{n_{\text{pix}}^{\text{SiPM}}}\right)} \times (1 - \varepsilon)\,, \tag{2.1}$$

where $n_{\text{pix}}^{\text{hit}}$ denotes the raw amplitude of a hit, $n_{\text{pix}}^{\text{SiPM}} = 96$ the total number of pixels in an SiPM array channel, and ε the crosstalk probability of the channel. The corrected cluster amplitude is given by the sum $n_{\text{p.e.}}^{\text{cluster}} = \sum n_{\text{p.e.}}^{\text{hit}}$. The crosstalk probability is determined from the deviation of Poissonian statistics in the light injection runs preceding the particle data runs [12].

The light yield increases with overvoltage for both curves due to the increasing photon detection efficiency. For higher overvoltages the corrected light yield starts to saturate whereas the raw cluster amplitudes keep increasing as the crosstalk probability increases.

Fig. 2.8 shows the raw cluster amplitudes as a function of the tilt angle α of the module. In general the increase of the path length inside the scintillator is reflected in an increase of the light yield. The actual path length inside the scintillator depends on both the angle and the crossing position of the charged particles because of the complicated fibre coverage

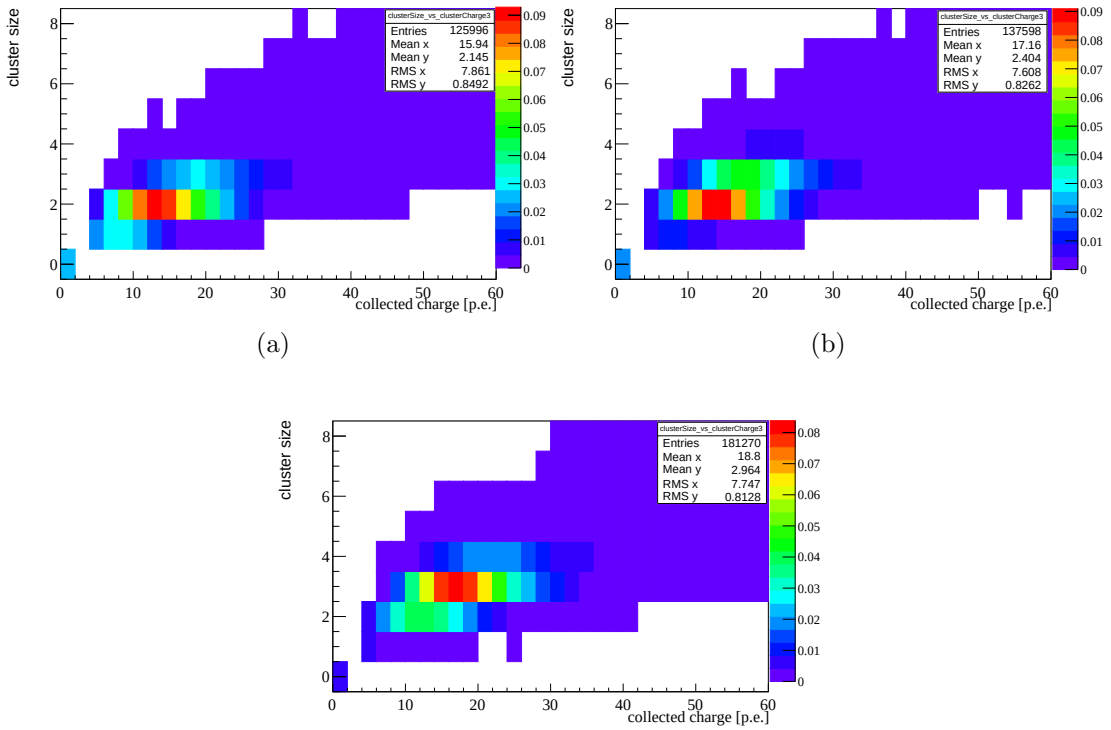

Figure 2.4: The cluster size plotted versus the cluster charge for tracks near the mirror at a module rotation of (a) 0 , (b) 10, and (c) 20 degrees with respect to the beam.

pattern. Therefore, the dependence is more complex than a $\cos^{-1}\alpha$ assumption, which is valid for a scintillator sheet.

2.2.2 Attenuation Length

A preliminary analysis of the light yield as a function of position for the HD1 and HD2 modules was done without the use of the two telescopes, but required that track hits were also found in the other three of the four modules. The HD1 and HD2 modules did not have mirrors attached, while Slayer and Coverlay did have mirrors. The mean number of photoelectrons for a cluster was determined by using thresholds of 1.5 for the seed, 0.5 for the neighbour and 2.5 for the sum.

The intensity of the light, given here as the mean number of detected photoelectrons N, is modelled by a double exponential which decreases with the distance from the excitation point:

$$N(x) = N_S e^{-x/\Lambda_S} + N_L e^{-x/\Lambda_L} \tag{2.2}$$

where Λ_S and Λ_L represent the short and long components, respectively. Λ_S will contain components of the light travelling through the cladding or other helical paths and

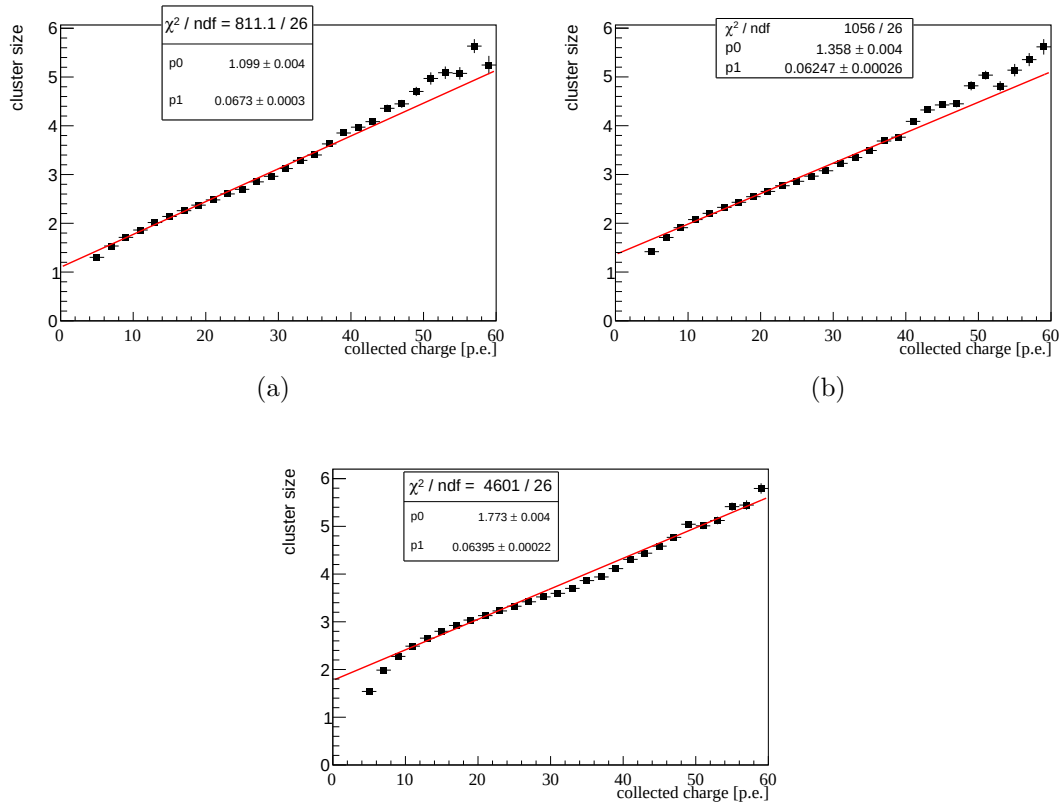

Figure 2.5: The mean cluster size plotted versus the cluster charge for tracks near the mirror at a module rotation of (a) 0 , (b) 10, and (c) 20 degrees with respect to the beam. The fit is a straight line, $y = p0 + p1 \cdot x$.

is of the order of few tens of centimetres when measured as the distance along the fibre axis. Λ_L contains the light propagating through core with few reflections is typically defined as the attenuation length for long fibres. Additionally, the attenuation length is strongly dependent on the wavelength of scintillation light, with short blue components and longer green components. N_S and N_L are the number of photoelectrons of each component at distance zero.

For single fibres, Kuraray suggests a single exponential fit from 1 to 3 metres[1] (distances at which the short component would be negligible) from the excitation point:

$$N(x) = N_0 e^{-x/\Lambda} \tag{2.3}$$

2.2.2.1 Modules without mirror

The attenuation length of modules without mirror, HD1 and HD2, were obtained by using a single exponential fit (from 1 to 3 m) and the function from eq. (2.2). The data and

[1] the fibre modules are only 2.5m in length

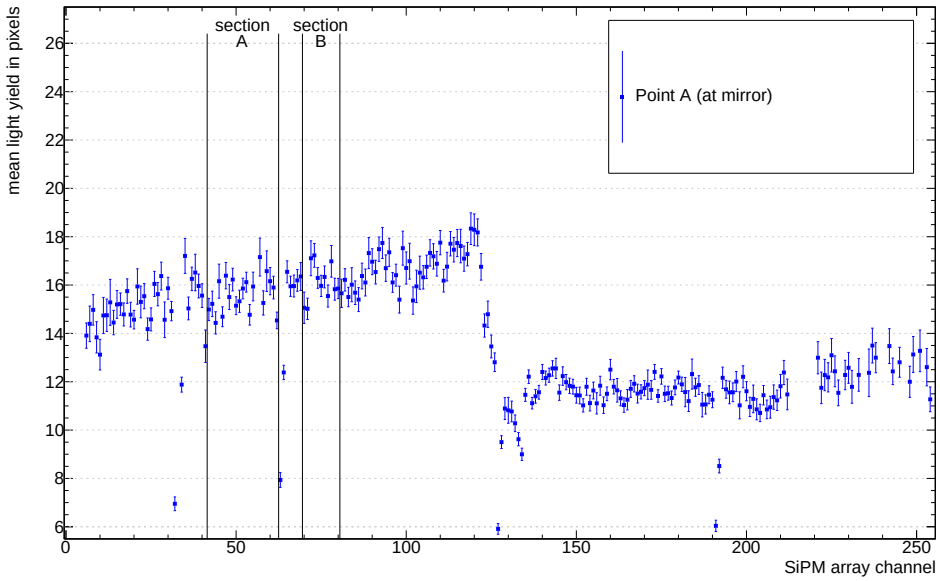

Figure 2.6: Mean cluster amplitude profile over the two SiPM arrays used to read out the module.

fit to the data are shown in Figures 2.9 and 2.10. Values of Λ=402 cm and 309 cm have been found for single exponential fits to the data for HD1 and HD2, respectively.

2.2.2.2 Modules with mirror

The attenuation length of the Slayer module was studied using tracks matched to the AMS ladder telescope. Fig. 2.11 shows the horizontal mean cluster amplitude profile together with a projection at position A (closest to the mirror). The auto calibration capabilities of the SiPMs (clearly defined photoelectron peaks) can be seen from the signal pealing at integer values (gray curve) once the gain factor has been divided out. The re-binned version of the curve (green) shows the expected Landau shape. Assuming a fixed reflectivity $R = 85\,\%$ for the mirror the curve

$$s(x) = s_0 \cdot \left(e^{-\frac{x}{\Lambda}} + R \cdot e^{-\frac{500\,\mathrm{cm}-x}{\Lambda}} \right), \tag{2.4}$$

where x denotes the distance to the readout side, is fitted in the range $x > 100\,\mathrm{cm}$ obtaining $\Lambda = 310\,\mathrm{cm}$.

2.2.3 Spatial Resolution

The single-point resolution is determined by comparing the distance between the AMS reference track extrapolated to the position of the fibre module and the position of the

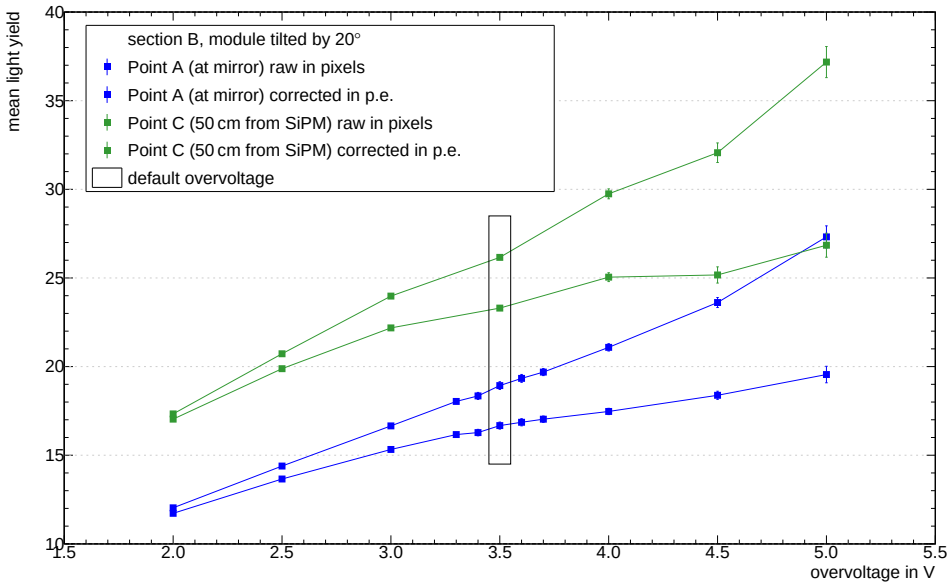

Figure 2.7: Raw and corrected cluster amplitudes as a function of the overvoltage at two distances to the readout side of the mat. The module was tilted by 20 ° during these scans.

reconstructed cluster. The width σ_{residual} of this distribution is the quadratic sum of the track uncertainty σ_{track} and the single point resolution σ_{SciFi}

$$\sigma_{\text{residual}} = \sqrt{\sigma^2_{\text{track}} + \sigma^2_{\text{SciFi}}} \approx \sigma_{\text{SciFi}}. \tag{2.5}$$

where the track resolution from the telescope is small relative to the SciFi and does not contribute much such that the residual is approximately the resolution of the scintillating fibre tracker and are used interchangeably. The residual is parametrized with a double Gaussian

$$\propto (1-f) \cdot e^{-\frac{1}{2}\left(\frac{x-\mu}{\sigma_{\text{inner}}}\right)^2} + f \cdot e^{-\frac{1}{2}\left(\frac{x-\mu}{\sigma_{\text{outer}}}\right)^2}, \tag{2.6}$$

where f denotes the percentage of σ_{outer}. It is found that the value is always between 6 % and 9 %. Assuming a single point resolution of 20 µm for the AMS ladders, the resolution of the telescope track extrapolated to the fibre module is calculated to be approximately 30 µm. It is 10 µm to 20 µm for the TimePix telescope. Here we only use the residual widths which still contain the uncertainty of the reference track. A more detailed study of the telescope properties is needed to subtract this uncertainty.

The two contributions to the double Gaussian can be combined to an effective resolution defined as

$$\sigma_{\text{eff}} = \sqrt{(1-f) \cdot \sigma^2_{\text{inner}} + f \cdot \sigma^2_{\text{outer}}}. \tag{2.7}$$

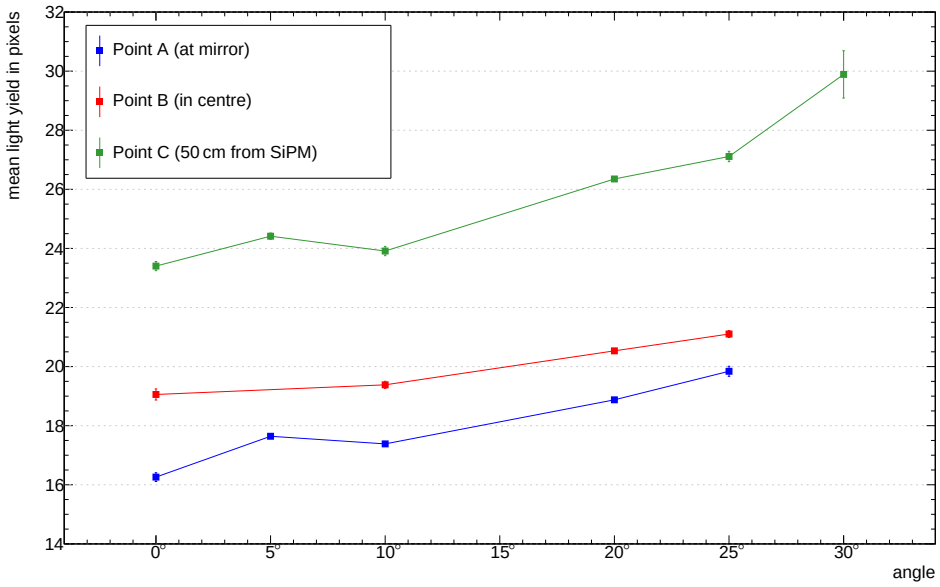

Figure 2.8: Raw cluster amplitudes as a function of the tilt angle of the module.

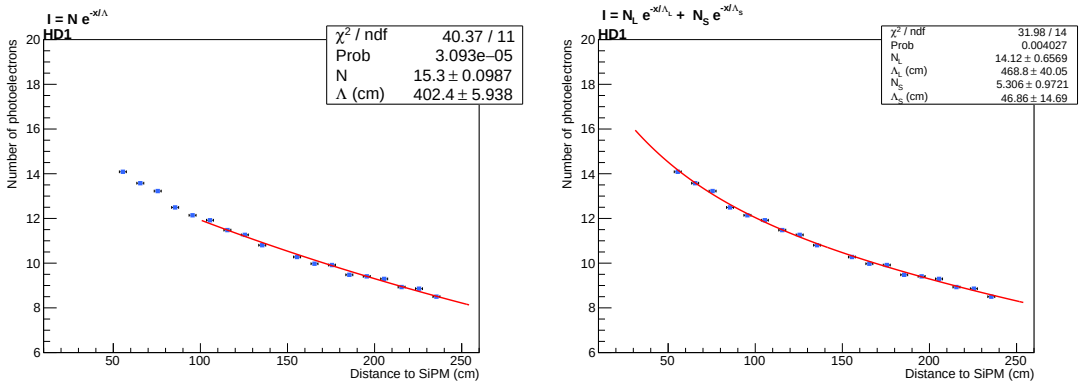

(a) (b)

Figure 2.9: Attenuation length measurement of the 5-layer mat module HD1. Picture (a) show the fit of an single exponential function from 1 to 3 m, and (b) corresponds to a fit using eq. 2.2.

Crosstalk and delta rays likely contribute to the wider outer Gaussian while the primary track produces the narrower inner distribution.

2.2.3.1 Analysis with TimePix tracks

For the determination of the spatial resolution, the residual of the SciFi cluster positions with respect to the reconstructed TimePix tracks are calculated where the TimePix tracks

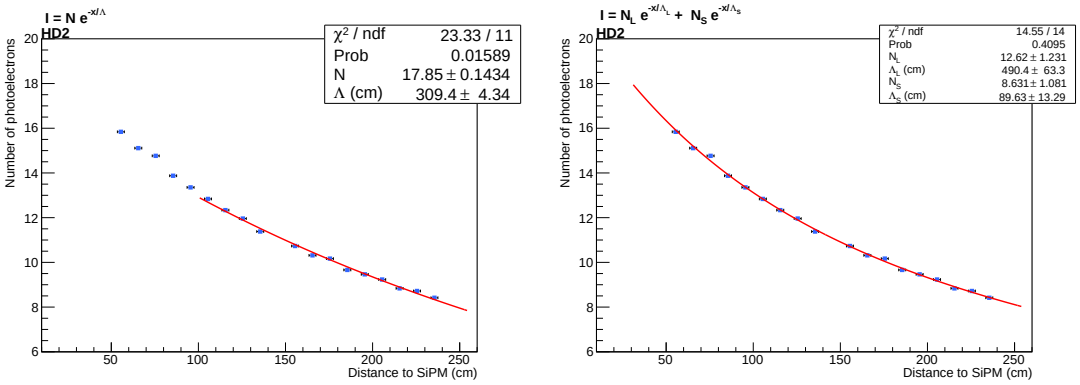

(a) (b)

Figure 2.10: Attenuation length measurement of the 5-layer mat module HD2. Picture (a) show the fit of an single exponential funtion from 1 to 2.5 m, and (b) corresponds to a fit using eq. 2.2.

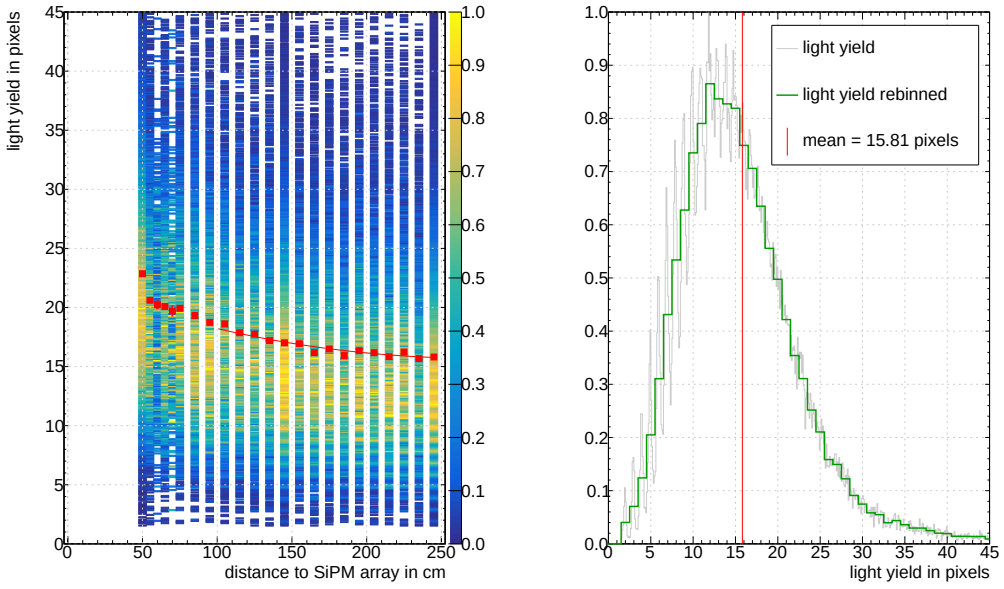

Figure 2.11: Cluster amplitude as a function of the distance to the readout side (left) and projection of the slice closest to the mirror (right) in section A.

are required to exhibit a track χ^2/ndof smaller than 4. Clusters are determined using foreseen LHCb thresholds of 2.5 for the seed, 1.5 for the neighbour and 4.0 for the sum. Tracks that are within the area of the gap between the dies of the SiPM or at broken channels are excluded. Additionally, the tracks are required to be correctly reconstructed by all SciFi modules except for the DUT (detector under test). The distributions of the

residuals using the charge-weighted mean and the Pacific-like hit-weighted mean[2] as the SciFi cluster position is shown in Fig. 2.12 (also in A.9 and A.10 in the appendix) for the three horizontal positions.

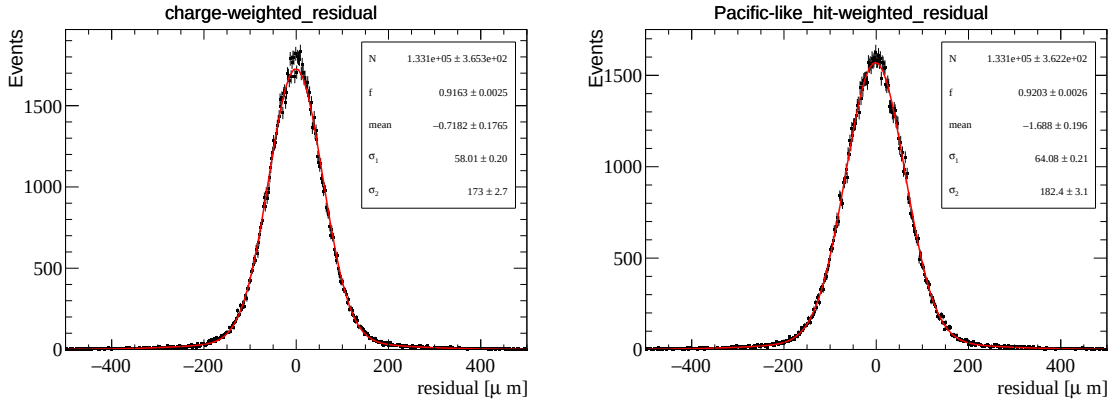

Figure 2.12: Charge-weighted (left) and Pacific-like hit-weighted(right) residual distributions of hits to the reconstructed TimePix track at the mirror.

Table 2.3 gives the results for the effective resolutions. Whereas the charge-weighted clustering benefits from an increase of total light yield, the resolution applying the Pacific-like hit-weighting one stays constant over the module. At the mirror, the charge-weighted resolution is better than (74.07 ± 0.58) µm and the hit-weighted resolution better than (79.78 ± 0.61) µm. These numbers are broader than a simple single Gaussian, as the tails contribute significantly to the position resolution. Studies revealed correlations between the tails and large clusters. When applying the clustering algorithm with splitting large clusters, the results are given on the bottom of Table 2.3. The effective width decreases by approximately 5 µm.

The dependence of the performance on an incident angle of the beam relative to the module is investigated by tilting the module away from the beam in steps of 10°. Tables 2.4 and A.6 (appendix) give the effective charge-weighted $\sigma_{eff,charge}$ and Pacific-like hit-weighted spatial $\sigma_{eff,Pacific}$ resolution as a function of an incident angle at the mirror and 50 cm from the SiPM.

The resolution is seen in Figure 2.13 to vary with the (a) cluster charge and (b) cluster size, typically becoming worse for wide clusters or large charge amplitude clusters (which are themselves correlated). The worse resolution, along with the wide clusters and greater charge lends weight to the hypothesis that the creation of additional ionizing secondary particles is depositing addition energy in the neighbouring fibres.

2.2.3.2 Analysis with AMS ladder tracks

Fig. 2.14 shows the effective resolution for the horizontal scan data set. It is notably constant at a value of 65 µm within 5 µm over the whole length of the module. The 12 −bit

[2]as described in Section **??**

Table 2.3: Effective charge-weighted $\sigma_{eff,charge}$ and Pacific-like hit-weighted spatial $\sigma_{eff,Pacific}$ resolution when neglecting the TimePix telescope resolution at the mirror, at the centre of the module and 50 cm from the SiPM

	at the mirror	centre	50 cm from SiPM
$\sigma_{eff,charge}$ [µm]	74.07 ± 0.58	73.14 ± 0.32	69.71 ± 0.41
$\sigma_{eff,Pacific}$ [µm]	79.78 ± 0.61	80.11 ± 0.33	80.91 ± 0.45
		split large Clusters	
$\sigma_{eff,charge}$ [µm]	68.68 ± 0.56	67.97 ± 0.25	63.22 ± 0.34
$\sigma_{eff,Pacific}$ [µm]	74.91 ± 0.53	74.71 ± 0.26	74.16 ± 0.38

Table 2.4: Effective charge-weighted $\sigma_{eff,charge}$ and Pacific-like hit-weighted spatial $\sigma_{eff,Pacific}$ resolution at the mirror as a function of an incident angle between the beam and the module

	0 °	10 °	20 °
$\sigma_{eff,charge}$ [µm]	74.07 ± 0.58	77.67 ± 0.60	88.51 ± 0.61
$\sigma_{eff,Pacific}$ [µm]	79.78 ± 0.61	82.84 ± 0.65	92.11 ± 0.66
		split large Clusters	
$\sigma_{eff,charge}$ [µm]	68.68 ± 0.56	71.14 ± 0.59	80.58 ± 0.55
$\sigma_{eff,Pacific}$ [µm]	74.91 ± 0.53	76.47 ± 0.59	84.23 ± 0.58

ADCs of the USB readout boards allow the simulation of the 2 bit PACIFIC readout by reducing the digital information artificially. An additional curve for this cluster positioning

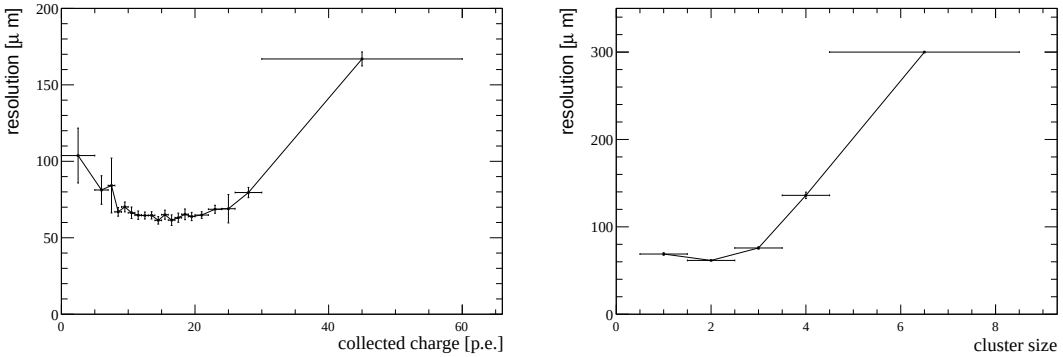

(a) (b)

Figure 2.13: The resolution of the fibre tracker plotted versus (a) cluster charge and (b) cluster size, for perpendicular tracks near the mirror

is shown. The resolution worsens by about 15 µm.

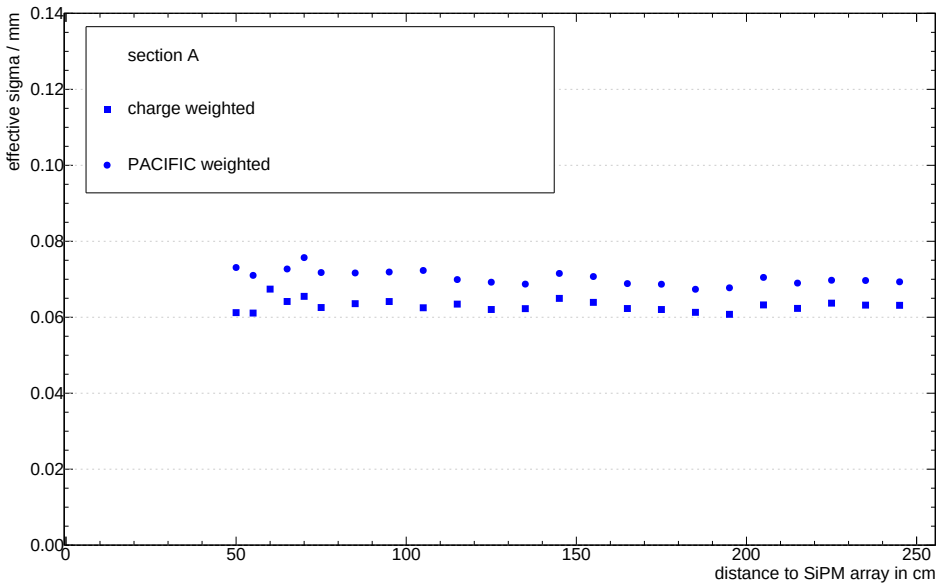

Figure 2.14: Effective resolution as a function of the position along the fibre mat for perpendicular incidence angle.

Fig. 2.15 shows the correlation between the inner resolution σ_{inner} and the light yield for all four modules. The five-layer modules HD1 and HD2 combine with the six layer DUT smoothly. Above about 15 pixels mean cluster amplitude the resolution does not improve much anymore. The CERN Coverlay mat is by far worse than the other modules. The same behaviour is also observed in the cluster widths. The mounting of the SiPM arrays on the coverlay module can explain both jumps in the data, which was found to be caused by a screw head creating a larger air gap than intended.

The effective resolution as a function of the overvoltage at point A and C can be seen in Fig. 2.16. All curves show a broad minimum around the default overvoltage of 3.5 V that will be used in the LHCb detector. The module is tilted by 20 °.

Fig. 2.17 shows an approximately linear increase of the resolution with the tilt angle. The linear stage used to position the fiber mats drifted with time and ambient temperature with respect to the telescope. Therefore, the necessary software alignment is hard to do for all data points and the stated resolutions are actually better. Despite this issue all determined resolutions are by far better than the design goal of 100 µm.

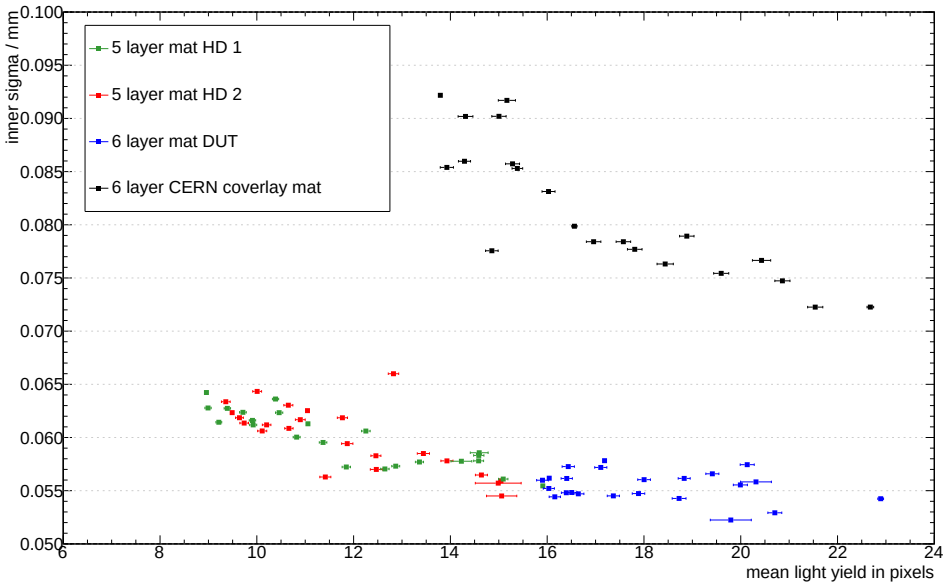

Figure 2.15: Inner resolution as a function of the mean raw cluster amplitude.

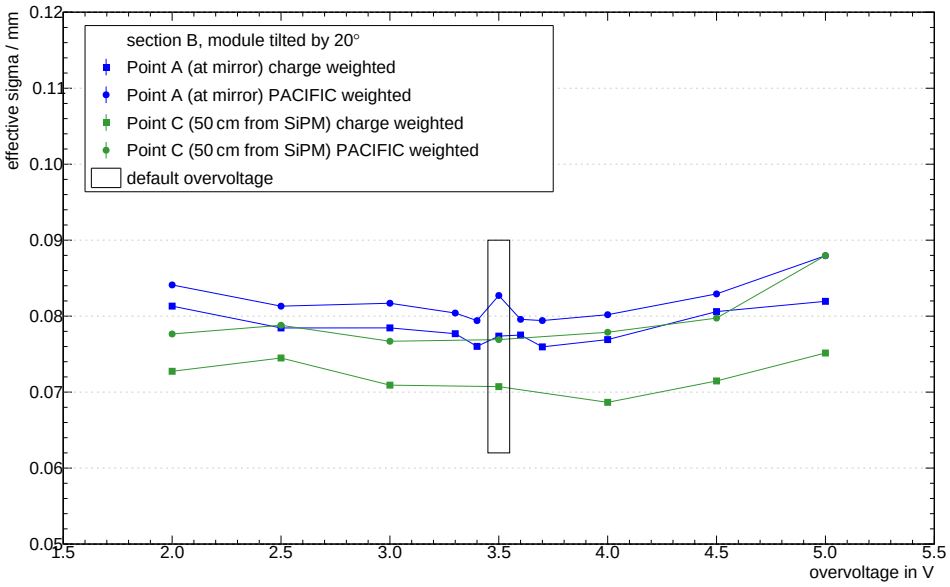

Figure 2.16: Effective resolution as a function of the overvoltage.

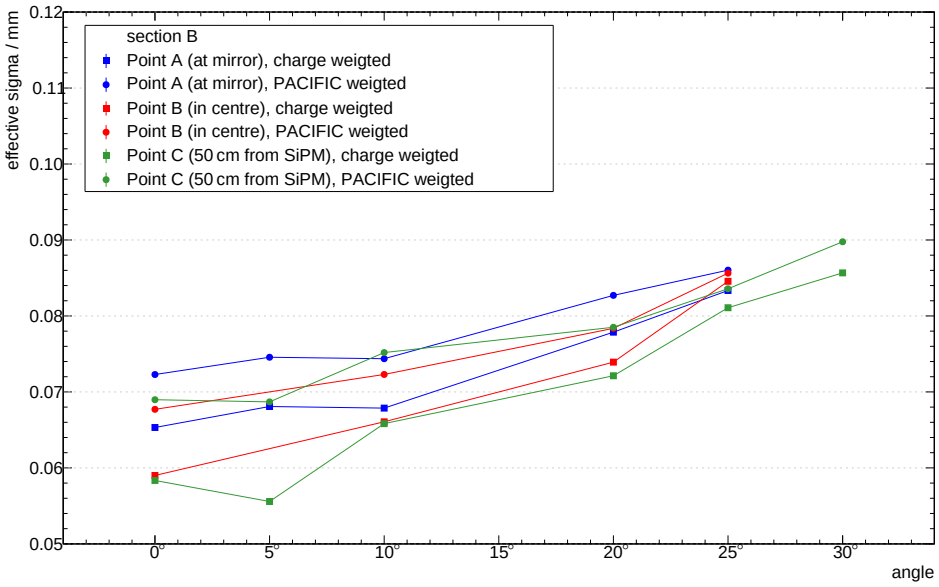

Figure 2.17: Effective resolution as a function of the tilt angle.

2.2.4 Hit Efficiency

The efficiency is determined by counting how often a particle passing through the fibre mat creates a cluster. The independent telescope track is used to determine the position of the particle passing through the fibre module and the hit efficiency is the fraction of matching tracks from the fibre module data. The hit efficiency of the 6-layer Slayer module is presented here as the detector under test (DUT).

2.2.4.1 Analysis with TimePix tracks

The single-hit efficiency is determined by the ratio of the number of correctly reconstructed fibre clusters to the number of predicted TimePix tracks. It depends on the applied cluster thresholds and on the allowed distance from the cluster to the reference track. Accepting all hits that are less than 5 channels away from the TimePix track, the left-hand side of Fig. 2.18 shows the single-hit efficiency as a function of the channel ID of the SiPM array for different seed thresholds. The beam traverses the module next to the mirror. The neighbour threshold is chosen to be 1.5 p.e. For illustration purposes channel 65 corresponds to the gap between the two dies[3]. For the gap, the efficiency decreases to about 45%.

To determine the efficiency away from the gap, a constant function is fit to the efficiency plateau of the channels left from the gap. The fit results are given in Table 2.18 and plotted against their corresponding thresholds on the right of Fig. 2.18. (Additional tables

[3]The SiPM array comprises two dies, each with 64 channels.

and plots can be found in Appendix A.2.) For the right-hand plots, the black data points have a sum threshold chosen to be equal to the seed threshold whereas for the blue point the sum threshold is 4.0 p.e. as it is expected to be chosen for the future SciFi.

The hit efficiencies with standard LHCb thresholds (1.5, 2.5, 4.0) for near the mirror, at the centre of the module and 50 cm from the SiPM can be found in Table 2.5. Also, the single-hit efficiency with standard LHCb thresholds for different angles at the mirror (Point A) are shown in Table 2.6.

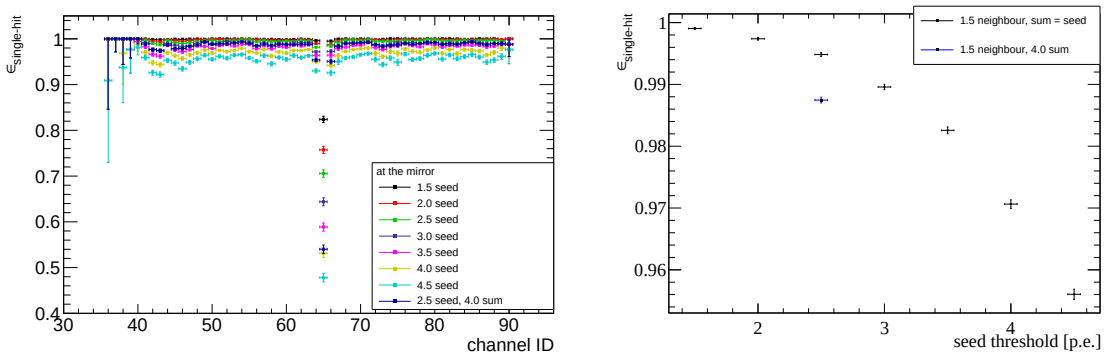

(a) (b)

Figure 2.18: Single-hit efficiency vs. SiPM channels ID (a) at the mirror. For illustration purposes channel 65 corresponds to the gap between the two dies. On the right, the efficiency at the plateau for channels away from the gap is plotted against the seed threshold.

Table 2.5: The hit efficiency for detecting matched TimePix telescope tracks near the mirror, at the centre of the module and 50 cm from the SiPM for the standard LHCb thresholds (1.5, 2.5, 4.0).

	at the mirror	centre	50 cm from SiPM
ϵ [%]	98.75 ± 0.05	99.30 ± 0.02	99.93 ± 0.01

Table 2.6: The single hit efficiency for the DUT at the mirror (Point A) for different angles for the standard LHCb thresholds (1.5,2.5,4.5).

	0 °	10 °	20 °
ϵ [%]	98.75 ± 0.05	99.56 ± 0.03	99.60 ± 0.02

2.2.4.2 Analysis with AMS ladder tracks

If a found cluster contains a hit within 3 channels distance to the predicted particle position, the event has passed the efficiency requirement. In order to minimize the effect of badly reconstructed events, which would degrade the efficiency, only clean events are selected for the analysis.

For this it is demanded that

1. there be exactly one cluster in the three double-sided stations of the AMS ladder telescope,
2. the χ^2 of the fitted track is smaller than 10 (having 6 clusters for four track parameters), and
3. there be maximally one cluster in each of the fibre modules.

The efficiency is calculated with the help of ROOT's TEfficiency class. Fig. 2.19 shows the vertical efficiency profile of the fibre module at a distance of 250 cm (point A), 145 cm (point B), and 50 cm (point C) from the readout side. The upper plot shows the efficiency using low cluster thresholds and the lower plot shows the efficiency using the standard cluster thresholds foreseen for the PACIFIC readout in the upgraded LHCb detector.

The efficiency is very close to one in the case of low thresholds. For LHCb thresholds the influence of the degraded light yield due to the badly aligned SiPM arrays is clearly reflected in the efficiency. The mean efficiency close to the mirror is 98.2 % in section A and 99.0 % in section B. The improved efficiency in section B is likely a result of the better alignment of the SiPM, as can be seen in Fig. 2.6. The hit efficiency is likely higher in the sections with even better light yield.

Fig. 2.20 shows the efficiency as a function of the position along the fibre mat within section A. The low threshold curve remains close to one, whereas the LHCb threshold curve shows a decrease to the value of 98.2 % towards the mirror as the light yield decreases.

Particles passing the detector under an angle increases the path length within the scintillator material. This leads to an increase in light yield and efficiency as seen in Fig. 2.21

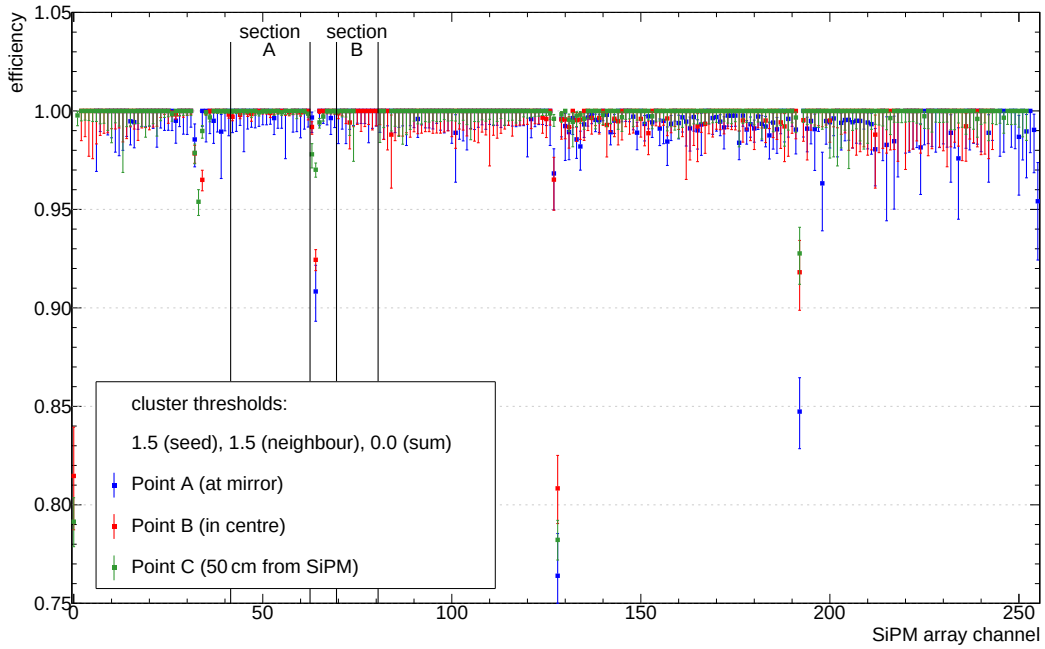

(a)

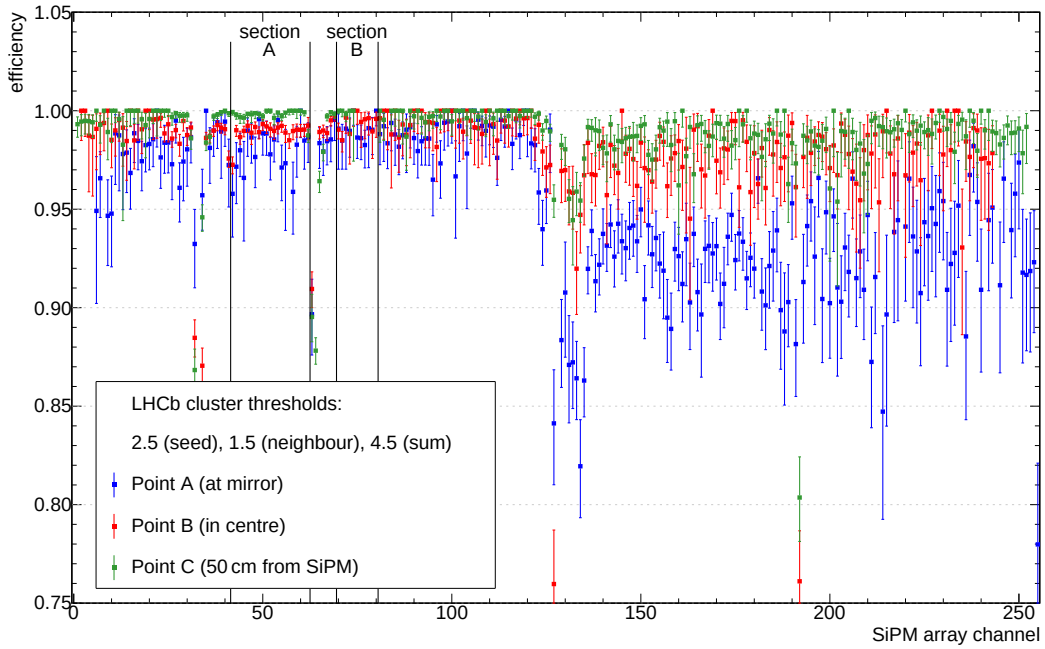

(b)

Figure 2.19: Vertical efficiency profile for low cluster thresholds (a) and for LHCb cluster thresholds (b) at three positions along the fibre mat.

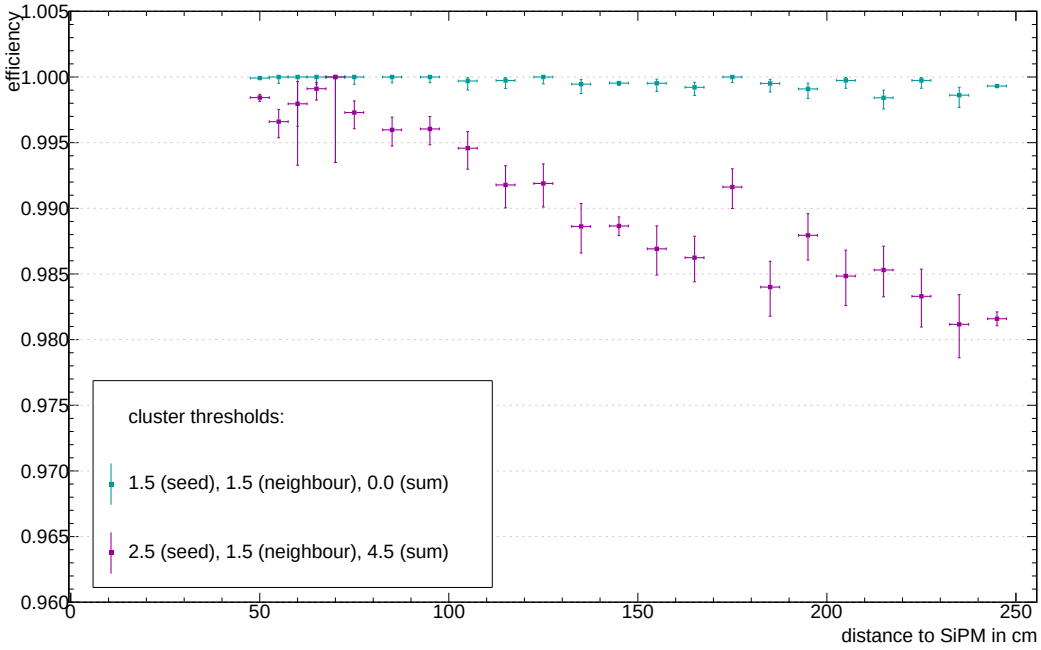

Figure 2.20: Efficiency as a function of the distance to the readout side of the module.

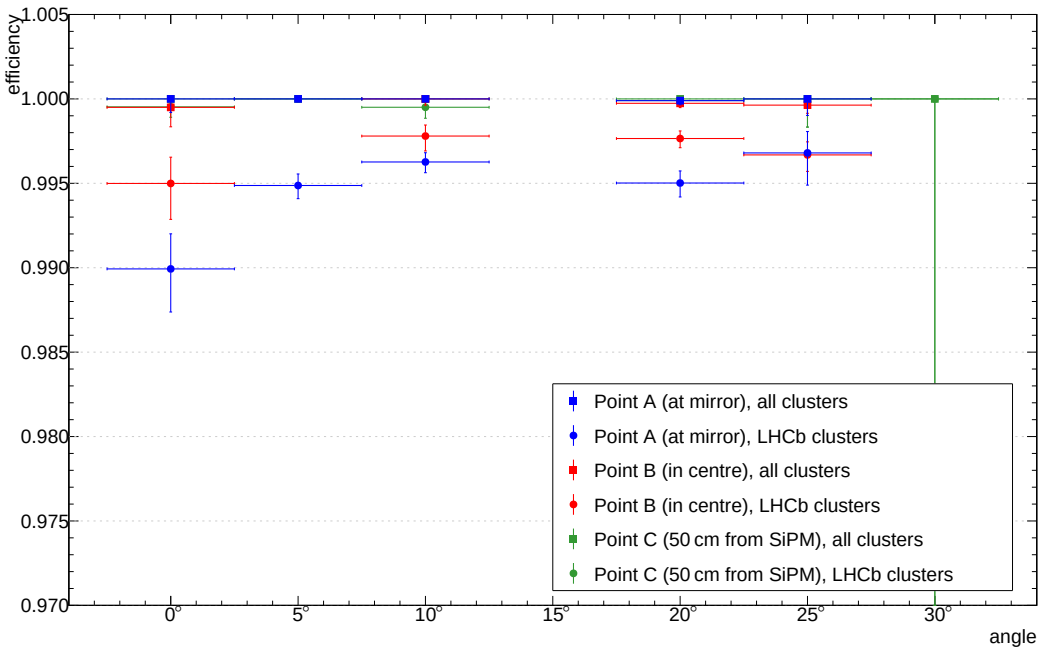

Figure 2.21: Efficiency as a function of the module tilt angle.

Chapter 3

Test Beam in November 2015

3.1 Experimental setup

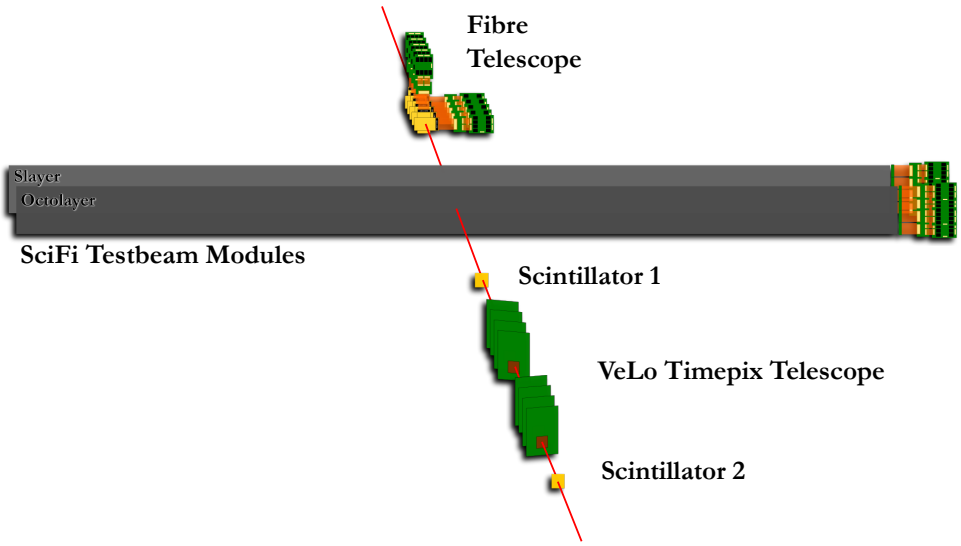

Figure 3.1: The relative detector layout with two test beam modules in H8 at the SPS in November 2015. The path of the beam is indicated by the red line.

The experimental setup of the test beam campaign in November 2015 is shown in 3.1. Two modules, Slayer and Octolayer, were equipped with four SiPM arrays in order to study the uniformity across the entire fibre mat. A description of the modules can be found in Sec. 1.3.2. Two external telescopes were used during this campaign to provide reconstructed particle tracks with a resolution much better than the DUTs. A newly constructed telescope made from small fibre mats was used in addition to the VeLo TimePix telescope(see Sec. 2.1.2). However, no tracks were used from the fibre telescope in this analysis and will not be described further. Only TimePix tracks have been used.

The data acquisition triggers were formed from a coincidence of two scintillators placed

fore and aft of the TimePix telescope, approximately 2 cm^2 each in size. As in the May testbeam, the SiPMs are readout by the SPIROC front-end boards which contain 4 to 8 EASIROC ASIC chips, described in Chapter 1. Each SPIROC card is connected to one of the eight uplinks of the USB-board DAQ which digitises the signal via a 12-bit ADC and provides fast and slow control to the front end cards.

3.2 Six-layer module irradiation

The SciFi detector is expected to operate up to an integrated luminosity of 50 fb^{-1} [2]. A FLUKA simulation [13, 14] describes the expected dose in the first tracking station after 50 fb^{-1} assuming a proton-proton cross section of 100 mb at $\sqrt{s}$=14 TeV. Fig. 3.2(a) shows the expected dose, which ranges from 35 kGy in the region close to the beampipe down to 50 Gy in the SiPMs region.

The six-layer-module has been characterised in both test beam campaigns (in May and November 2015). In October 2015 the module has been irradiated with a beam of 24 GeV protons in the CERN PS IRRAD facility [15]. The irradiation procedure started on the 26th of October at 17:00 and lasted a total of 27 hours [16]. The aim of the irradiation was to reproduce on the module the same dose profile as in the real LHCb detector after 50 fb^{-1}. The module was positioned such that the beam centre will hit 32 mm from the lower module edge, as illustrated in Fig. 3.2(b).

Aluminium strips were fixed on the module in order to perform a dosimetry analysis after the irradiation. During irradiation aluminium is activated to sodium isotopes, ^{24}Na and ^{22}Na. Dosimetry is based on the determination of the number of protons which hit the aluminium by evaluating the ^{22}Na activity, which was measured after the irradiation with a Germanium detector. The dose absorbed by polystyrene can be obtained from the number of protons that hit the strips and it is shown in Fig 3.3 as a function of the position along the module.The data points are exclusively based on the analysis of the ^{22}Na activity. The data was fitted with a sum of three exponential functions (red line). The plots include also the targeted dose as predicted by the FLUKA calculations (black line). The ratio plots show the ratio of the measured and target doses. Within the uncertainties, the measured dose profile matches well the targeted distribution. An additional 10% uncertainty reflects an inconsistency between two Ge-spectrometers used for the dose Na-activity measurements. At positions below 20 cm, the module was under-irradiated by about 20 %–30 % while for positions above 50 cm the measured results trend to a 30 %–40 % overdose. The irradiation can be considered as successful in the sense that it has reproduced a dose distribution which comes very close to the one expected in the final SciFi detector.

A much more detailed description of the irradiation can be found in [16].

3.3 Data Analysis

Where required, only tracks from the TimePix telescope have been used in order to determine the light yield, hit efficiency and position resolution.

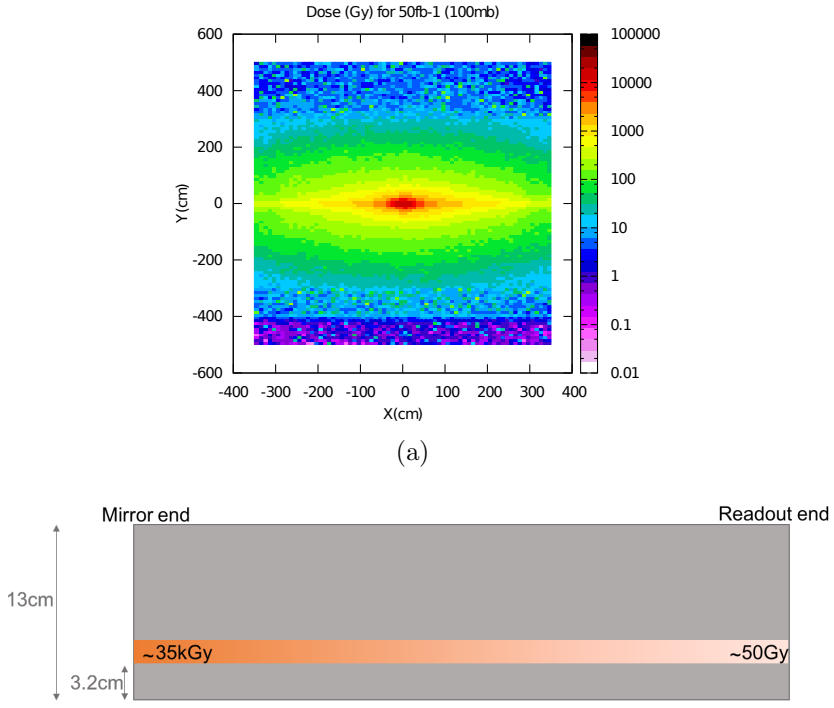

Figure 3.2: (a) The expected dose in the first tracking station of the SciFi Detector after an integrated luminosity of 50 fb^{-1} [2]. (b) An illustration of the location of the irradiated region within the module.

3.3.1 Light yield of irradiated module

The 6-layer module was placed in the SPS beam approximately one week after the irradiation at the PS, described above. The height of the module was adjusted on a linear table such that data could be collected for the majority of the channels across the module (the fibre axes are horizontal to the floor in the test beam). The nominal clustering algorithm was used to find clusters and determine the total light yield per cluster in the irradiated and non-irradiated regions. From previous irradiation studies and analyses [17–19], a 40 % loss in light yield at the mirror is expected from the LHCb-Upgrade dose profile after 50 fb^{-1} of integrated luminosity. The light yield will be greater further away from the mirror.

The light yield, when positioning the beam near the mirror, can be seen in Figure 3.4. The loss of light seen at the centre of the irradiated region, decreasing from 15 to below 5 photoelectrons, corresponds to approximately 70 % loss, and is much larger than what was expected. Given the severity of the apparent problem, several checks were made after the beam test to ensure that there were no miscalculations or mistakes in the dose measurement. No errors were found. Following the test beam, the module was placed into a buffer zone for irradiation materials for one month before being transported to the

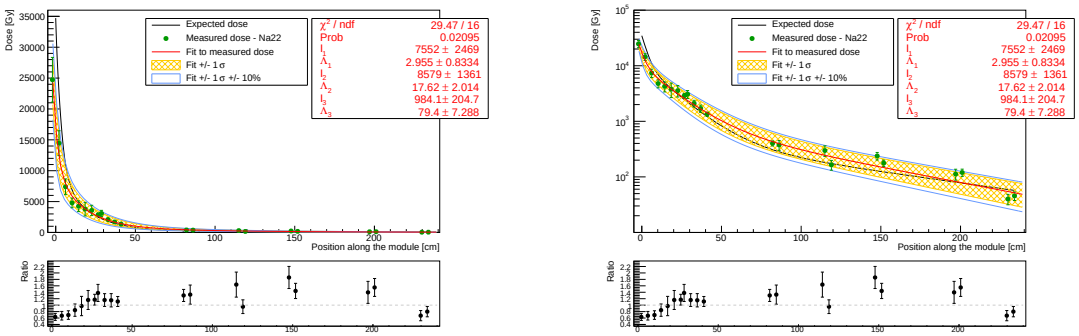

(a) Linear scale

(b) Logarithmic scale

Figure 3.3: Comparison of the expected and measured dose along the module. The left edge (position = 0 cm) corresponds to the mirror end. The black line represents the targeted dose on the module. The data points are the values of the dose measured with ^{22}Na. The data points were fitted with a sum of three exponential functions. The $\pm 1\sigma$ envelope is drawn as a yellow shaded area. The blue lines represent an additional $\pm 10\,\%$ uncertainty. The ratio plots show the ratio of the measured and target doses.

University of Heidelberg for additional measurements in the lab.

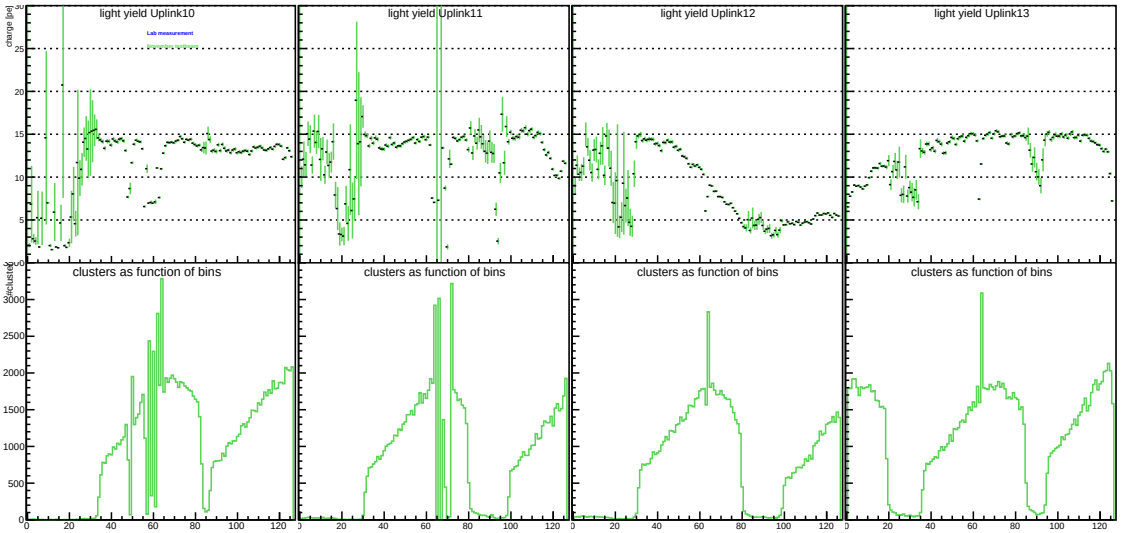

Figure 3.4: (top row) The mean light yield in each array across the module. The region on the right of Uplink 12 with a lower light yield corresponds to the irradiation beam spot. (bottom row) The location of the clusters from multiple measurements corresponding to the beam spot at different heights.

In Heidelberg, light yield measurements were made using a Sr-90 beta source. It had

been previously found that the beta source provides a similar light yield / cluster as the test beam. However, cluster sizes from the beta source tend to be consistently larger in width due to the mean path that the beta particle travels before stopping in the scintillator trigger placed below the test beam module. An additional 1 mm of PVC is placed above the trigger to stop very low energy betas and maintaining a more uniform dE/dx per beta particle. The entire module including carbon fibre skins, honeycomb cores, fibre mat and additional glue corresponds to approximately 4 mm equivalent of plastic. The light yield observed in Heidelberg using a beta source is shown in Figure 3.5. It can be seen that in the unirradiated regions, the light yield is approximately the same. However, in the centre of the irradiated region, the light yield has recovered and shows a light loss of approximately 40 %, similar to the predictions from previous irradiation measurements of individual fibres. Histograms showing the light yield distributions for several channels in the most irradiated part and unirradiated regions, in the test beam and in the lab with a beta source, are shown in Figure 3.6. From the overlapping location of the photopeaks, it is clear that it is not a result of a difference in the applied SiPM overvoltage or gain miscalibration. It appears that the irradiation damage has recovered in the two months between the testbeam and lab measurements. This is not entirely unexpected, as annealing of scintillating fibres has been reported previously in the literature.

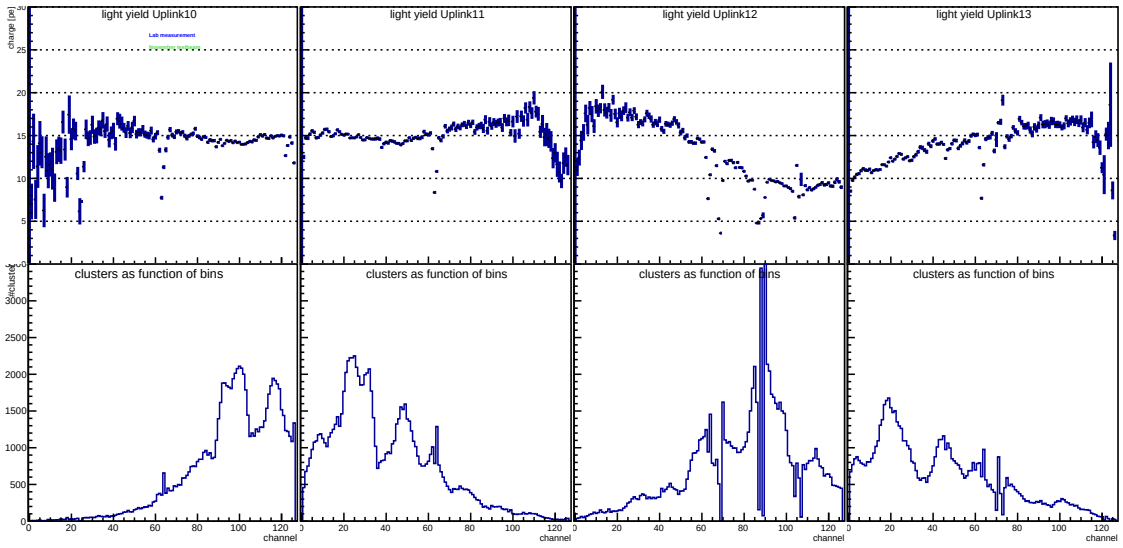

Figure 3.5: (top row) The mean light yield in each array across the module. The region with a lower light yield corresponds to the irradiation beam spot width. (bottom row) The location of the clusters from multiple measurements corresponding to the placement of the beta source above the module.

It was decided to remove the mirror on half of the irradiated section and compare the light yield to previous measurements of un-mirrored modules to try and disentangle any damage to the mirror or degradation of the optical glue used to bond the mirror. Further inspection of the module for mechanical damage to the mirror found no obvious damage

from a visual inspection. However, during the removal of the mirror section, it was found to be loosely bound and easily detached once sliced at the center of the irradiated beam spot. It is uncertain whether the mirror mechanics contributed to the loss of light yield during the tests. Further tests on mirror samples glued to scintillator to study the loss of light due to the degradation of the transmission of the mirror glue showed only minor transmission losses on the order of 1-2 % [6], [5].

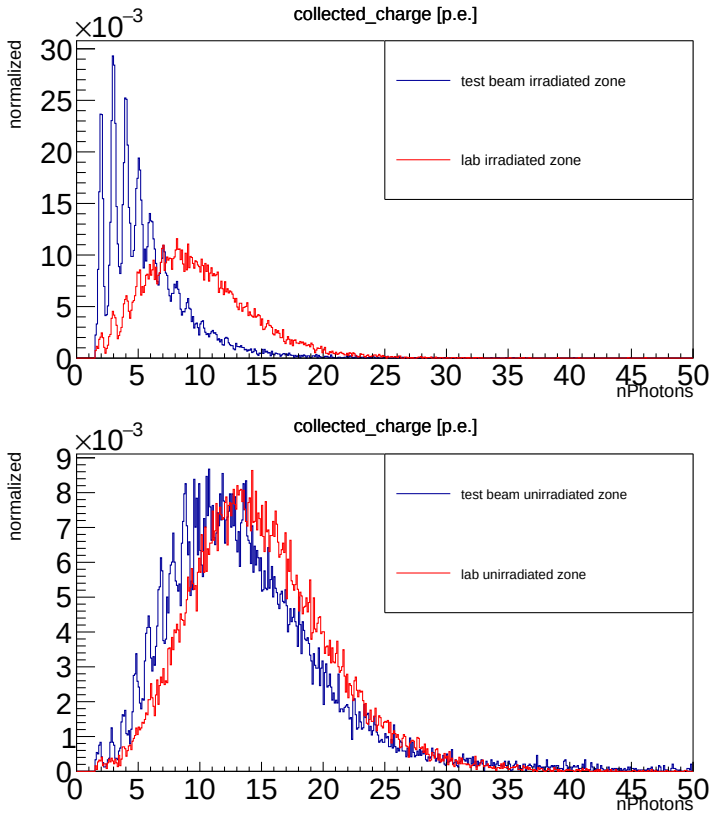

Figure 3.6: (top figure) The light yield measured in the test beam and in the lab with a beta source several channels of the most irradiated region (bottom figure) The light yield measured in the test beam and in the lab in the unirradiated region.

Given the unexpected low light yield, the hit efficiency and position resolution were not measured in the following sections. It is planned to re-machine and attach a new mirror to the irradiated module and conduct further test beam measurements on the module in October 2016. The additional measurements below regarding resolution and hit efficiency refer only to unirradiated parts of the 6-layer module. The 8-layer module is unirradiated.

3.3.2 Spatial Resolution

The methods used to determine the spatial resolution of the 6-and 8-layer module for the data of the November 2015 test beam are equivalent to the ones described in Sec. 2.2.3,

which are used to analyse the data of the test beam in May 2015. The spatial resolution is determined from the distribution of the residuals of the SciFi cluster positions with respect to the reconstructed TimePix tracks. Only TimePix tracks which exhibit a track χ^2/ndof smaller than 4 are considered. The SciFi clusters are determined using thresholds of 2.5 for the seed, 1.5 for the neighbour and 4.5 for the sum. These values refer to the minimum number of photo-electrons required to form the cluster. Tracks which lie inside the area of the gap between the SIPM dies or a broken channel are excluded. Tracks used for the determination of the spatial resolution for one of the two modules are required to be correctly reconstructed in the other module.

The distributions of the residuals for the 8-layer and the 6-layer module, using the charge-weighted mean and the Pacific-like hit-weighted mean as the SciFi cluster position are shown in Fig. 3.7 and 3.8, also in A.11 and A.12 in the appendix, for the two horizontal positions. The sum of two Gaussian functions with their widths σ_i weighted with the fractions f and $(1-f)$ of the respective Gaussian is fitted to the distributions of the residuals. Neglecting the small resolution of the TimePix telescope, the effective resolution σ_{eff} is determined as the squared sum of the widths σ_i weighted with their fraction:

$$\sigma_{eff} = \sqrt{f \cdot \sigma_1^2 + (1-f) \cdot \sigma_2^2} \tag{3.1}$$

The results for the spatial resolutions for the 6-layer and the 8-layer module are summarized in Table 3.1 for 0° and 10° angle with respect to the SPS beam.

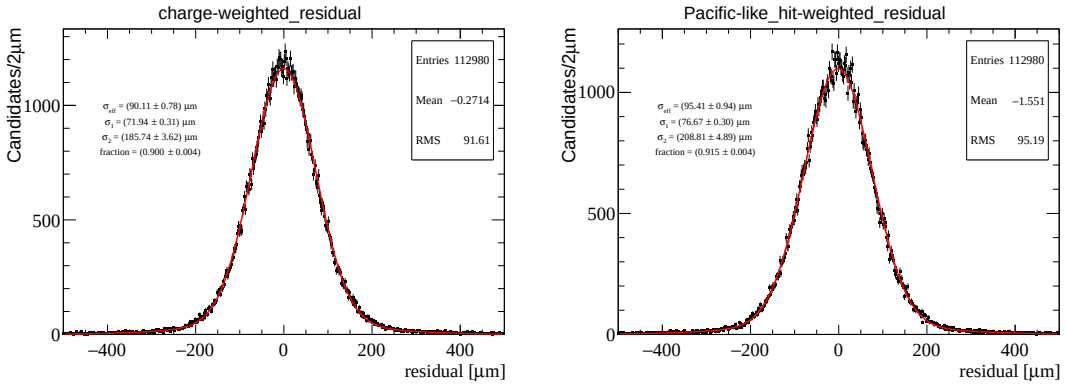

(a) (b)

Figure 3.7: Charge-weighted (a) and Pacific-like hit-weighted (b) residual distributions of hits to the reconstructed TimePix track at the mirror for the 8-layer module.

3.3.3 Hit Efficiency

The techniques used to determine the single-hit efficiency are described in Sec. 2.2.4. To obtain comparable results with the May 2015 test beam, all hits that are less than 5 SciFi

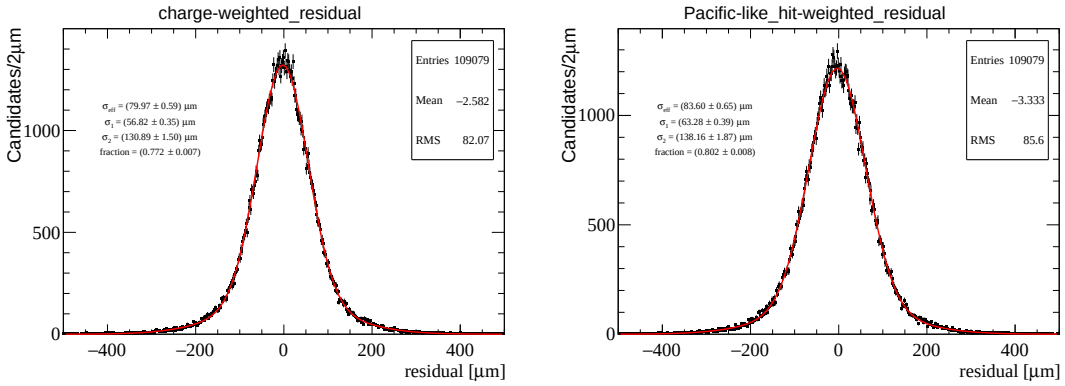

(a) (b)

Figure 3.8: Charge-weighted (a) and Pacific-like hit-weighted (b) residual distributions of hits to the reconstructed TimePix track at the mirror for the 6-layer module.

Table 3.1: Effective charge-weighted $\sigma_{eff,charge}$ and Pacific-like hit-weighted spatial $\sigma_{eff,Pacific}$ resolution for both modules at the mirror (A) and 50 cm from the the SIPM (C), as a function of an incident angle between the beam and the respective module.

	(A) 0°	(A) 10°	(C) 0°	(C) 10°
6-layer module				
$\sigma_{eff,charge}$ [µm]	79.97 ± 0.59	70.87 ± 1.09	77.46 ± 0.72	66.17 ± 0.90
$\sigma_{eff,Pacific}$ [µm]	83.60 ± 0.65	74.88 ± 1.13	86.94 ± 0.98	74.92 ± 1.10
8-layer module				
$\sigma_{eff,charge}$ [µm]	90.11 ± 0.78	88.61 ± 1.38	97.14 ± 0.95	81.61 ± 1.34
$\sigma_{eff,Pacific}$ [µm]	95.41 ± 0.94	91.63 ± 1.55	106.05 ± 1.28	88.26 ± 1.51

channels away from the extrapolated TimePix track are accepted. The left hand side of Fig. 3.9 and Fig. A.14 (Appendix) shows the hit efficiency for the 6 and 8 layer modules, respectively, as function of the channel ID of the SIPM array for different seed thresholds. The hit efficiency for each set of thresholds is determined by a single parameter fit that is applied to the respective distribution of efficiencies over the channels. The fit range is chosen such that dead channels and the gap between SIPM dies are excluded. The right hand side of the figures shows the fitted values for the hit efficiency as a function of the applied seed threshold. The hit efficiency for the fibre mats using the standard LHCb thresholds (1.5, 2.5, 4.5) are summarised in Table 3.2.

The obtained values for the hit efficiency of the 6-layer module are summarized in Table A.10 (near the mirror) and A.11 (near the SIPM) in the Appendix. For the 8-layer module the values are given in Table A.12 (mirror) and A.13 (SIPM), also in the Appendix.

The slightly lower hit efficiencies compared to the May testbeam in the 6-layer module can be attributed to the slightly higher Sum threshold applied (4.5 vs 4.0 photoelectrons) in the clustering algorithm. A strange effect was noticed in the data analysis, compared to the May 2015 analysis. The hit efficiency drops at 10 degrees near the mirror and increases near the SiPM for both the 6 and 8 layer modules, compared to the 0 degree data. Given that the increased light yield should increase the hit efficiency, the lower observed value is not expected. The statistical uncertainties are much smaller than the difference, and as such, some systematic effect must be playing a roll, possibly from the telescope tracks.

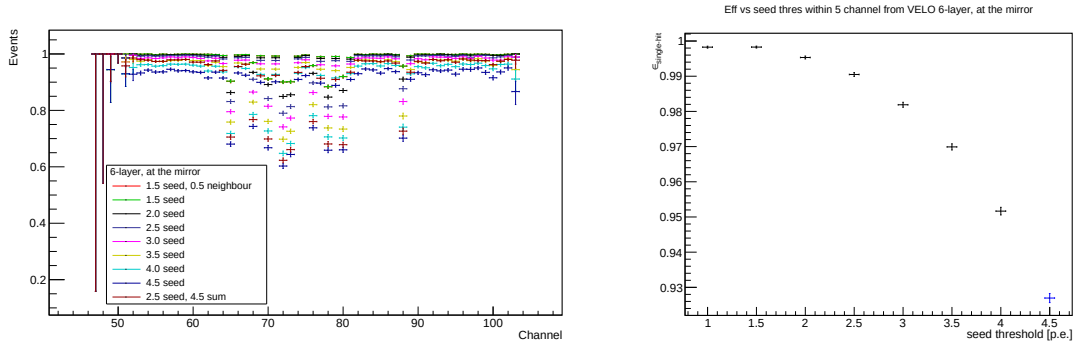

(a) (b)

Figure 3.9: Single-hit efficiency vs. SiPM channels ID (a) at the mirror. On the right, the efficiency at the plateau for channels away from the gap is plotted against the seed threshold. Both plots correspond to the 6-layer module.

Table 3.2: Effective charge-weighted $\sigma_{eff,charge}$ and Pacific-like hit-weighted spatial $\sigma_{eff,Pacific}$ resolution for both modules at the mirror (A) and 50 cm from the the SIPM (C), as a function of an incident angle between the beam and the respective module.

	(A) 0°	(A) 10°	(C) 0°	(C) 10°
6-layer module				
ϵ [%]	98.03 ± 0.11	97.82 ± 0.08	99.74 ± 0.04	99.92 ± 0.02
8-layer module				
ϵ [%]	98.24 ± 0.06	97.94 ± 0.09	99.75 ± 0.03	99.85 ± 0.03

Chapter 4

Conclusions

After two successful testbeam campaigns, it was seen that the light yield and hit efficiency of the scintillating fibre mats are sufficient for the tracking needs of the LHCb upgrade. Using 2014 Hamamatsu SiPM arrays and aluminised mylar foil mirrors, a mean light yield of 16 p.e. was found at the mirror with a hit efficiency of 98.7% and a position resolution better than 85 micron in the X-axis. Improvements in the PDE of the next generation of SiPMs, and improved mirror reflectivity, will improve the performance in the early running of the detector and mitigate some of the expected loss in performance of the detector due to radiation damage.

After annealing, the radiation damage expected after 50 fb^{-1} of integration luminosity will result in a 40% loss of signal.

It was seen that the curren system of readout electronics are well suited to the measurement of the light yield, hit efficiency and spatial resolution measurements of the scintillating fibre mats. The TimePix and AMS silicon ladder telescopes are both able to provide precision particle tracking such that the location on the fibre mats can be found with a resolution much smaller than the intrinsic fibre mat resolution.

The 8-layer mat was shown to be a viable solution to the "bump-problem" with a hit efficiency comparable to the 6-layer mat, and a resolution better than 95 micron at the mirror. However, the gains would not outweigh the reduction in signal to noise.

4.1 Acknowledgments

We would like to acknowledge the excellent support of the CERN SPS technical staff, and the cooperation of the other participating LHCb detector groups, during the setup and throughout the test beam campaign. Their contributions ensured a successful campaign and we are grateful.

Appendices

Appendix A

Additional material

A.1 Mat Winding continued...

For this the end of the fibre mat has been scanned. The resulting image has been analysed with a pattern recognition sofware to determine the position of the fibres. After this the distance between two neighbouring fibres and the distance between two fibre layers can be measured.

For the six layer mat the results are presented in Fig. A.1. The distance between two neighbouring fibres should represent the given thread of the winding wheel. This fibre mat has been produced on a winding wheel with a 275 µm pitch. The results reflect this very precisely. The mean for every layer is always around this given pitch. The standard deviation is rising with increased layer of fibres. This leads to a worse guidance in the higher fibre layers. But all this standard deviations are below 10 µm. The perfect distance between two layers can be calculated to 208.791 µm (d_{fibre}=250 µm, pitch=275 µm, without glue in between the layers). The results for this fibre mat are very comparable with the perfect distance between two fibre layers.

The same measurements have been done with the eight-layer-mat. The distance between two neighbouring fibres should represent the pitch of 350 µm of the used winding wheel. The histogram in Fig. A.2(a) show a mean of 350.3 µm with a standard deviation of 13.9 µm. The distance between two adjacent fibres for every layer can be found in Tab. A.1. The mean is always around 350 µm and the standard deviation in an expected range.

The distance between two fibre layers has been measured as well using an optical scanner and patern recongnition software. The resulting histograms can be found in Fig. A.2(b). The distance was measured to 182.7 µm with a standard deviation of 10.16 µm. The result is similar to the expected value and within allowed tolerances.

A.1.1 Casting

After winding, the fibre mat itself is a very fragile object an can be broken easily. To avoid this, a casting is necessary. Both mats have been casted with different methods. The six-layer-mat was embedded in a thin coating of glue (see Fig. A.3(a)). For this the

Table A.1: Mean and standard deviation σ for every layer for the eight-layer-mat. An increasing standard deviation leads to a worse guidance of the fibres in higher layers.

Layer	Mean / µm	σ / µm
1	350.3	11.3
2	350.3	13.4
3	350.3	13.4
4	350.3	13.5
5	350.2	13.6
6	350.2	14.7
7	350.5	15.9
8	350.2	14.8

mat has been placed in a special casting jig which was filled with glue. To align the mat correctly, pin holes in the jig were designed. A detailed description can be found in die EDR report [3]. This method is very time and work consuming, so that a different casting method has been followed. The eight-layer-mat has been casted with a 0.025 mm thin light-tight foil (see Fig. A.3(b)). This foil is glued to both sides of the fibre mat and has some gaps for the pins. This fibre mat was the first one casted with this method. During first light measurements it got clear, that not enough light reaches the SiPMs, and the needed light calibration of the SiPM arrays was not possible. Due to this the SiPM arrays were misaligned intentionally, such that the light could reached the SiPM via the endpiece directly.

A.2 Hit Efficiency Cont...

A.2.1 Analysis with TimePix tracks

A.2.2 Analysis with AMS ladder tracks

In Fig.A.6 the efficiency within section A is plotted as a function of the raw mean cluster amplitude as determined in Sec. 2.2.1.3 for all four fiber modules, using AMS ladder tracks. The curve shows a smooth transition of the light yield s of the modules, which is parametrized by

$$\varepsilon(s) = 1 - 10.1 \cdot e^{-0.39s}.$$

Below roughly 12 pixels or 90% efficiency, a rapid drop begins.. (*Editors note: the 5-layer modules contain a 3:2:3:2... column structure in the fibre matrix, compared to the 3:3:3:3...matrix structure in the 6-layer mats. The 5-layer mats are expected to have a worse hit efficiency from this structure for the same mean light yield as the 6-layer.*)

The efficiency also increases with the overvoltage due to both the increasing photon detection efficiency and the increasing crosstalk probability. Fig. A.7 shows the curves for

Table A.2: The single hit efficiency for a given seed, neighbour and sum threshold for the DUT at the mirror (A). The text in bold is the foreseen thresholds for the LHCb Upgrade.

Seed	Neighbour	Sum	Hit Eff.
1.5	1.5	1.5	0.9991 ± 0.0001
2.0	1.5	1.5	0.9974 ± 0.0002
2.5	1.5	1.5	0.9948 ± 0.0003
3.0	1.5	1.5	0.9896 ± 0.0004
3.5	1.5	1.5	0.9826 ± 0.0005
4.0	1.5	1.5	0.9706 ± 0.0007
4.5	1.5	1.5	0.9560 ± 0.0008
2.5	**1.5**	**4.0**	0.9875 ± 0.0005

Table A.3: The single hit efficiency for a given seed, neighbour and sum threshold for the DUT at the centre of the module(B). The text in bold is the foreseen thresholds for the LHCb Upgrade.

Seed	Neighbour	Sum	Hit Eff.
1.5	1.5	1.5	0.9996 ± 0.0001
2.0	1.5	1.5	0.9987 ± 0.0001
2.5	1.5	1.5	0.9975 ± 0.0001
3.0	1.5	1.5	0.9943 ± 0.0002
3.5	1.5	1.5	0.9905 ± 0.0002
4.0	1.5	1.5	0.9820 ± 0.0003
4.5	1.5	1.5	0.9726 ± 0.0004
2.5	**1.5**	**4.0**	0.9930 ± 0.0002

Table A.4: The single hit efficiency for a given seed, neighbour and sum threshold for the DUT 50 cm from the SiPM (C).

Seed	Neighbour	Sum	Hit Eff.
1.5	1.5	1.5	0.9998 ± 0.0001
2.0	1.5	1.5	0.9997 ± 0.0001
2.5	1.5	1.5	0.9996 ± 0.0001
3.0	1.5	1.5	0.9994 ± 0.0001
3.5	1.5	1.5	0.9992 ± 0.0001
4.0	1.5	1.5	0.9980 ± 0.0001
4.5	1.5	1.5	0.9964 ± 0.0002
2.5	**1.5**	**4.0**	0.9993 ± 0.0001

the positions close to the mirror and close to the readout within channel section B.

A.3 May 2015 Analysis cont...

Table A.5: Average light yield 50 cm from the SiPM as a function of an incident angle between the beam and the module. Not corrected for crosstalk.

	0°	10°	20°
mean light yield [p.e.]	23.93 ± 0.54	23.75 ± 0.11	26.69 ± 0.16
median light yield [p.e.]	22.29± 0.50	22.07 ± 0.10	24.92 ± 0.10
		split large Clusters	
mean light yield [p.e.]	23.52 ± 0.53	23.24 ± 0.11	25.72 ± 0.09
median light yield [p.e.]	22.29 ± 0.50	22.01 ± 0.09	24.62 ± 0.09

Table A.6: Effective charge-weighted $\sigma_{eff,charge}$ and Pacific-like hit-weighted spatial $\sigma_{eff,Pacific}$ resolution 50 cm from the SiPM as a function of an incident angle between the beam and the module

	0°	10°	20°
$\sigma_{eff,charge}$ [μm]	69.71± 0.41	70.84 ± 0.92	83.09± 0.61
$\sigma_{eff,Pacific}$ [μm]	80.91± 0.45	80.58 ± 1.14	88.65± 0.69
		split large Clusters	
$\sigma_{eff,charge}$ [μm]	63.22± 0.34	64.14 ± 1.10	73.59± 0.54
$\sigma_{eff,Pacific}$ [μm]	74.16± 0.38	74.20 ± 1.18	79.54± 0.59

A.3.1 single-hit efficiency

A.4 November 2015 Analysis continued...

The performance of the modules under an inclination of 10° is investigated. Table **??** shows the effective spatial resolution for the 6-layer and the 8-layer module under an incident angle of 10°, at the mirror and near the SIPM. The single-hit efficiency for both modules under the same inclination is shown in Table A.9.

Table A.7: The single hit efficiency for a given seed, neighbour and sum threshold for the DUT at the mirror (A) for different angles. The text in bold is the foreseen thresholds for the LHCb Upgrade.

Seed	Neighbour	Sum	0°	10°	20°
1.5	1.5	1.5	0.9991 ± 0.0001	0.9997 ± 0.0001	0.9996 ± 0.0001
2.0	1.5	1.5	0.9974 ± 0.0002	0.9991 ± 0.0001	0.9990 ± 0.0001
2.5	1.5	1.5	0.9948 ± 0.0003	0.9982 ± 0.0002	0.9982 ± 0.0001
3.0	1.5	1.5	0.9896 ± 0.0004	0.9958 ± 0.0003	0.9940 ± 0.0002
3.5	1.5	1.5	0.9826 ± 0.0005	0.9921 ± 0.0004	0.9893 ± 0.0003
4.0	1.5	1.5	0.9706 ± 0.0007	0.9833 ± 0.0005	0.9751 ± 0.0004
4.5	1.5	1.5	0.9560 ± 0.0008	0.9719 ± 0.0007	0.9610 ± 0.0005
2.5	**1.5**	**4.0**	0.9875 ± 0.0005	0.9956 ± 0.0003	0.9960 ± 0.0002

Table A.8: The single hit efficiency for a given seed, neighbour and sum threshold for the DUT 50 cm from the SiPM (C) for different angles.

Seed	Neighbour	Sum	0°	10°	20°
1.5	1.5	1.5	0.9998 ± 0.0001	0.9997 ± 0.0002	0.9998 ± 0.0001
2.0	1.5	1.5	0.9997 ± 0.0001	0.9997 ± 0.0002	0.9998 ± 0.0001
2.5	1.5	1.5	0.9996 ± 0.0001	0.9997 ± 0.0002	0.9997 ± 0.0001
3.0	1.5	1.5	0.9994 ± 0.0001	0.9996 ± 0.0002	0.9995 ± 0.0001
3.5	1.5	1.5	0.9992 ± 0.0001	0.9995 ± 0.0002	0.9993 ± 0.0001
4.0	1.5	1.5	0.9980 ± 0.0001	0.9986 ± 0.0003	0.9982 ± 0.0001
4.5	1.5	1.5	0.9964 ± 0.0002	0.9975 ± 0.0003	0.9969 ± 0.0002
2.5	**1.5**	**4.0**	0.9993 ± 0.0001	0.9996 ± 0.0002	0.9996 ± 0.0001

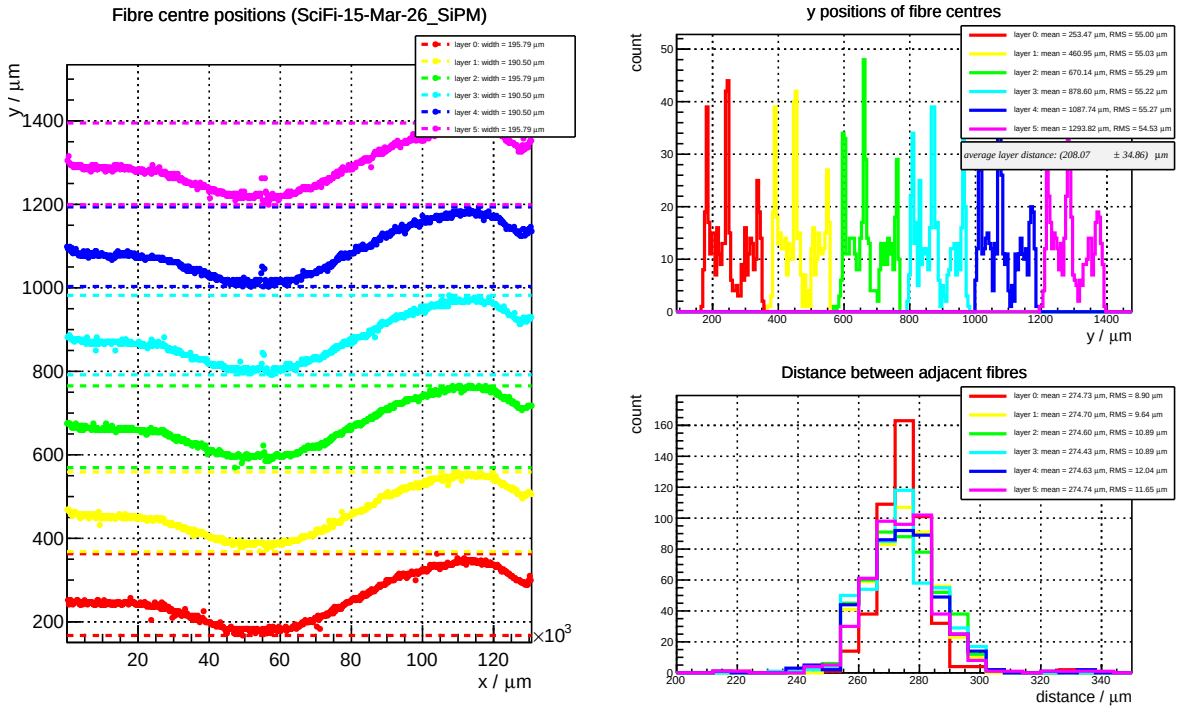

(a)

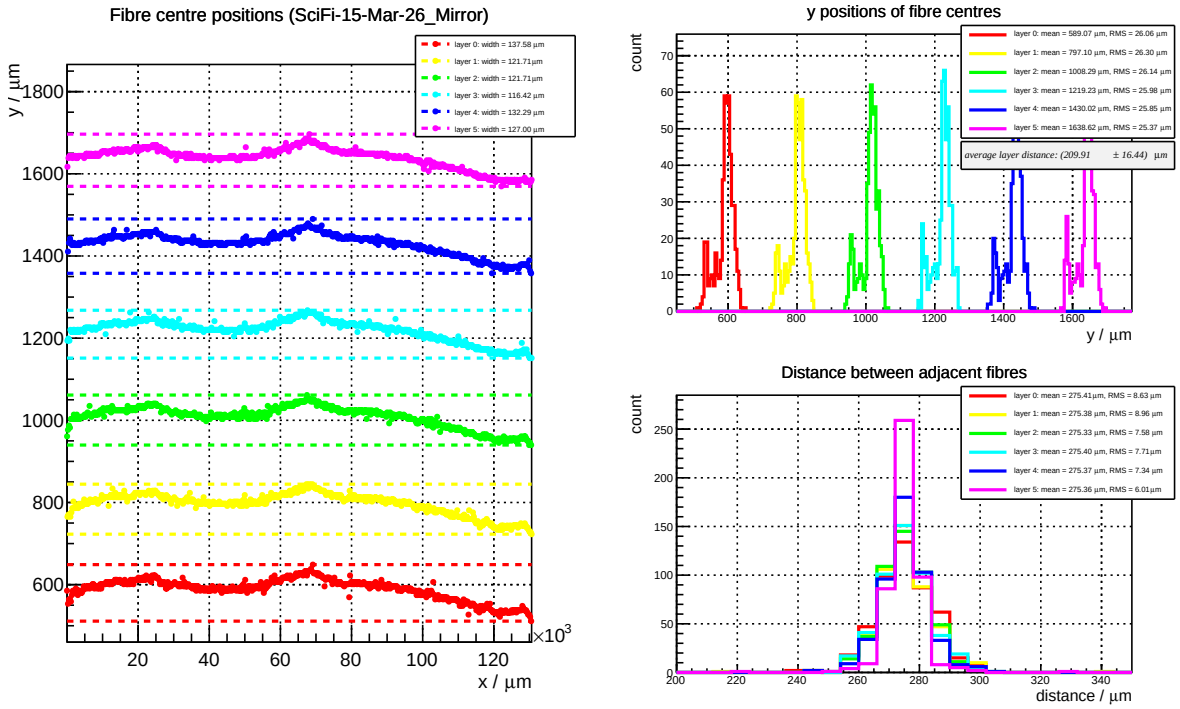

(b)

Figure A.1: Result of the cross section scan of the six-layer-mat. Both sides (SiPM (a) and Mirror (b)) have been scanned and analysed. The distance between two adjacent fibres and the distance between the fibre layers are shown.

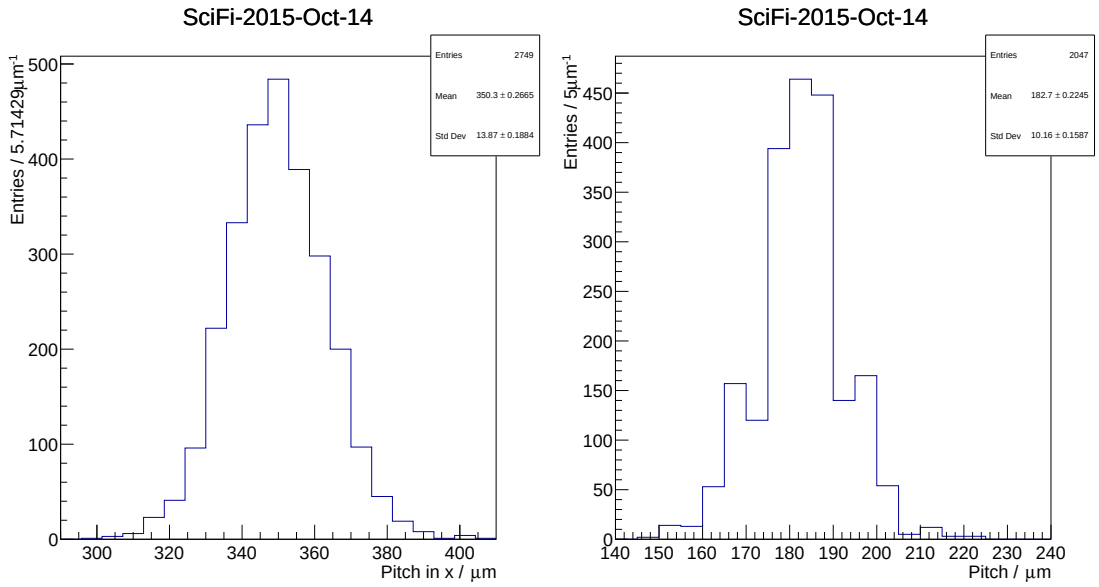

(a) (b)

Figure A.2: Results of the cross-section-scan of the eight-layer-mat. (a) The distance between two adjacent fibres are measured to 350.3 µm with a standard deviation of 13.9 µm. (b) The distance between two fibres layers was measured to 182.7 µm with a standard deviation of 10.16 µm.

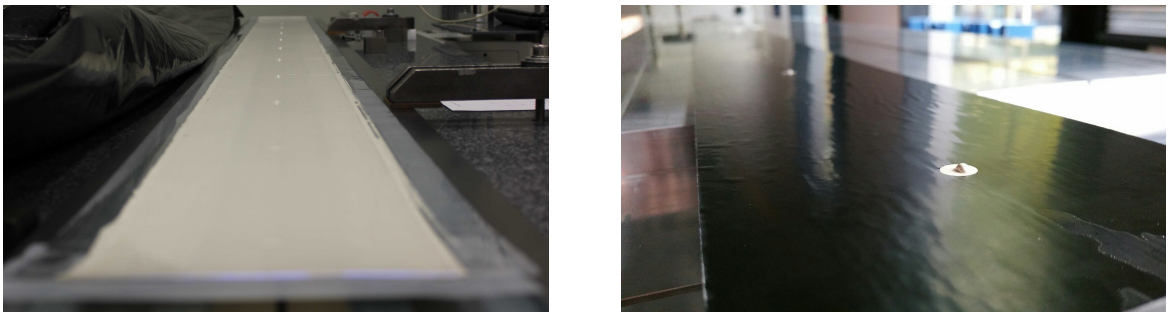

(a) (b)

Figure A.3: Examples for casted mats. (a) Glue-casted fibre mat. The protective glue layer is 80 µm thick. (b) Fibre mat casted with a 0.025 mm thin light tight foil.

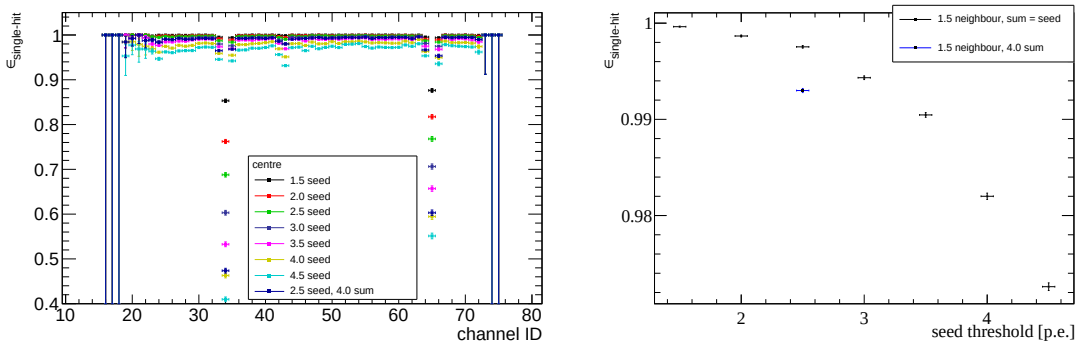

Figure A.4: Single-hit efficiency vs. SiPM channels ID (left) at the centre of the module. For illustration purposes channel 65 corresponds to the gap between the two dies. Channel 34 is a dead channel. On the right,the efficiency at the plateau for channels away from the gap is plotted against the seed threshold.

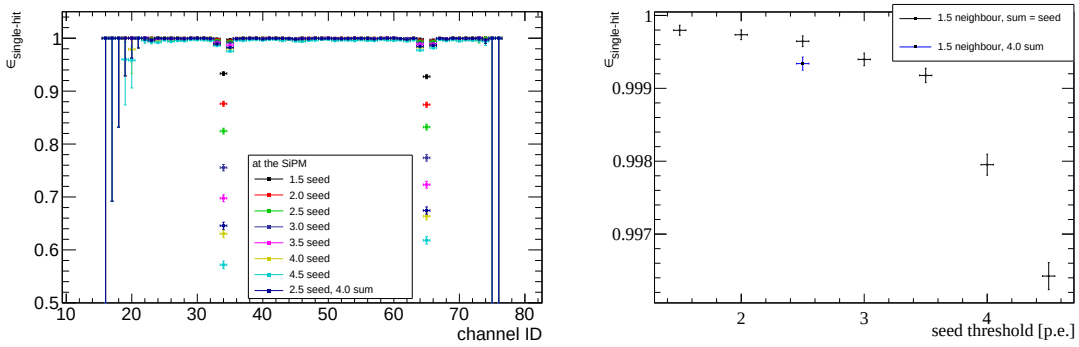

Figure A.5: Single-hit efficiency vs. SiPM channels ID (left) 50cm from the SiPM. For illustration purposes channel 65 corresponds to the gap between the two dies. Channel 34 is a dead channel. On the right,the efficiency at the plateau for channels away from the gap is plotted against the seed threshold.

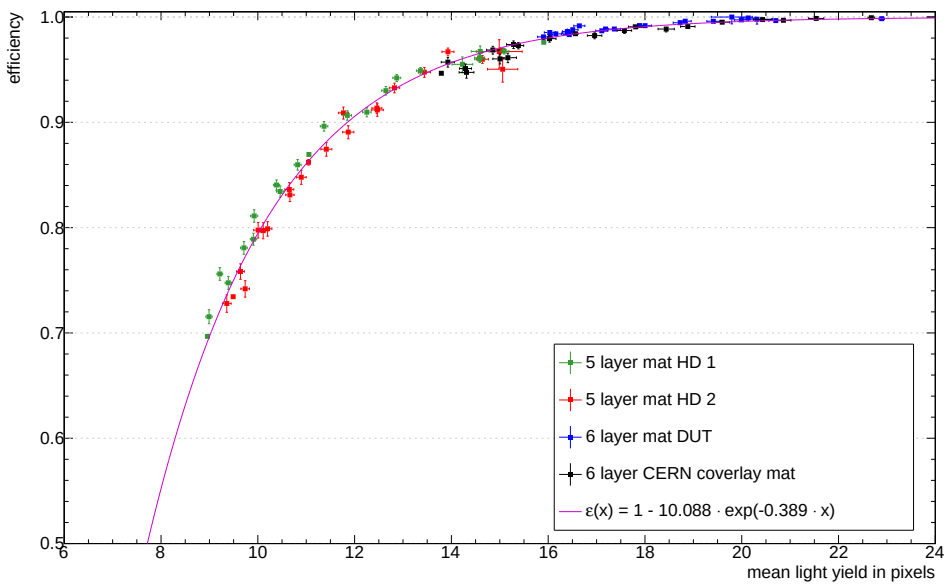

Figure A.6: Correlation of efficiency and light yield for all four fiber modules. (*Editors note: the 5-layer modules contain a 3:2:3:2... column structure in the fibre matrix, compared to the 3:3:3:3...matrix structure in the 6-layer mats. The 5-layer mats are expected to have a worse hit efficiency from this structure for the same mean light yield as the 6-layer.*)

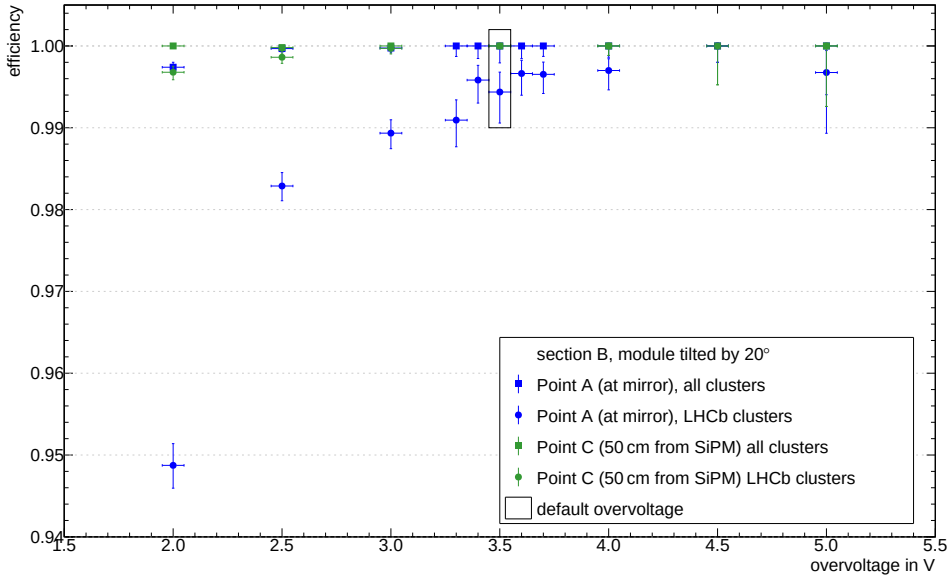

Figure A.7: Efficiency as a function of the overvoltage. Note that the module was tilted by 20° in contrast to the previously shown efficiency values.

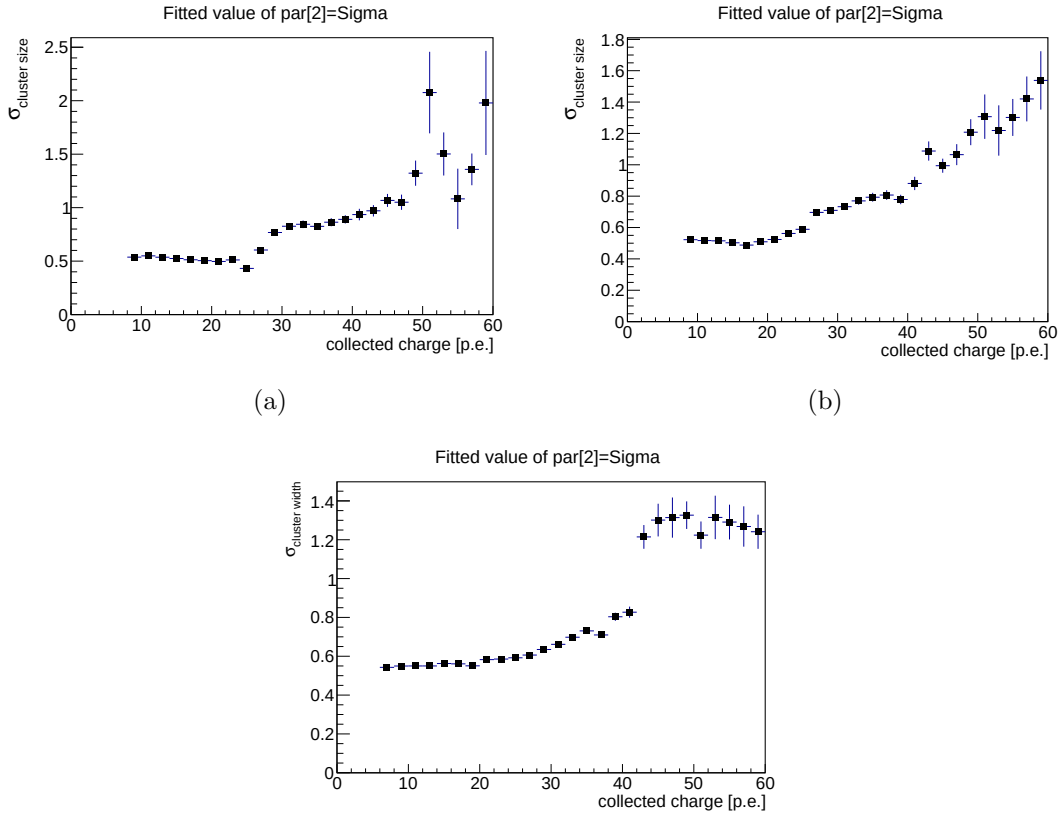

Figure A.8: The spread (sigma) of the cluster size plotted versus the cluster charge for tracks near the mirror at a module rotation of (a) 0 , (b) 10, and (c) 20 degrees with respect to the beam.

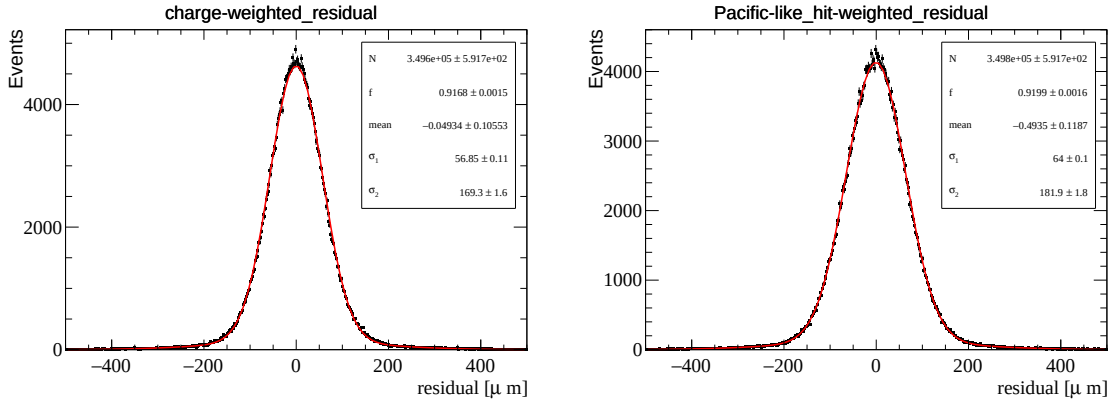

Figure A.9: Charge-weighted (left) and Pacific-like hit-weighted(right) distributions of hits to the reconstructed TimePix track at the centre of the module.

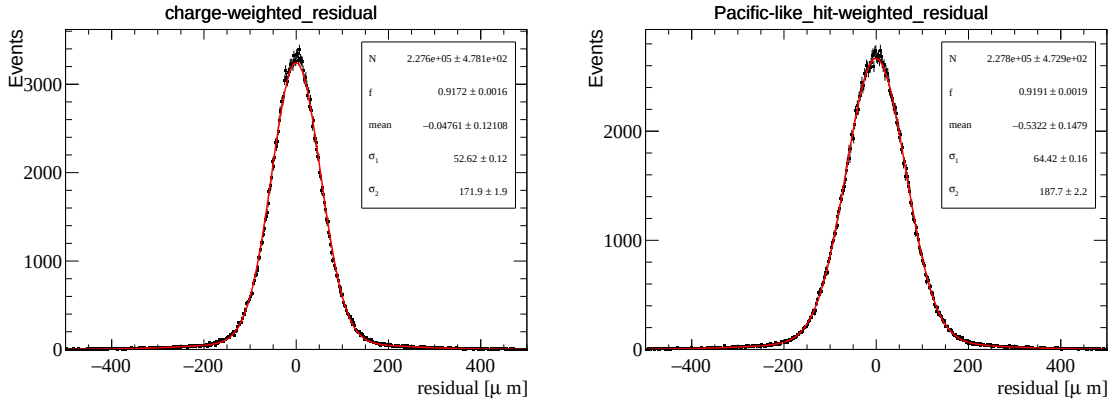

Figure A.10: Charge-weighted (left) and Pacific-like hit-weighted(right) distributions of hits to the reconstructed TimePix track 50 cm from the SiPM.

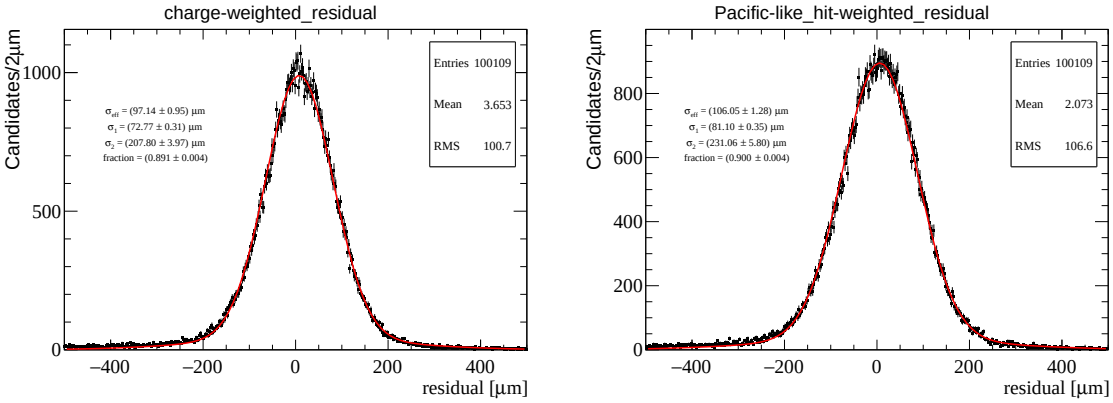

Figure A.11: Charge-weighted (left) and Pacific-like hit-weighted(right) residual distributions of hits to the reconstructed TimePix track 10 cm from the SIPM for the 8-layer module.

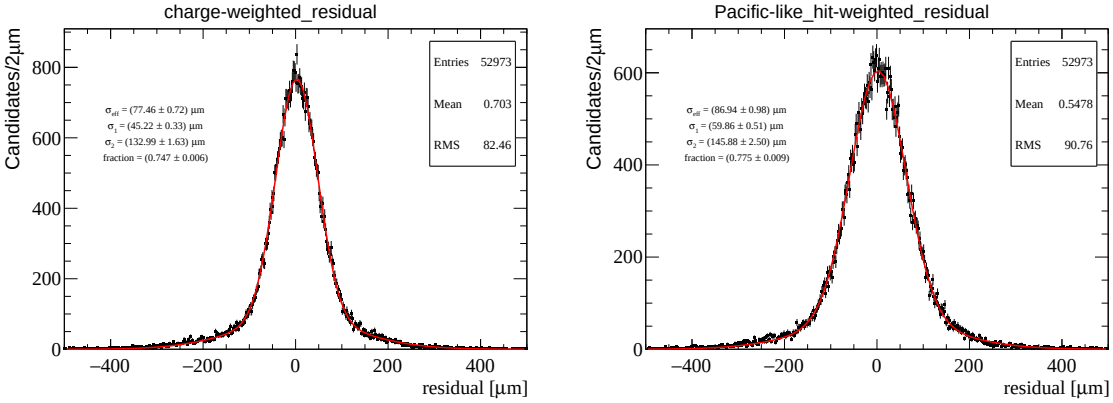

Figure A.12: Charge-weighted (left) and Pacific-like hit-weighted(right) distributions of hits to the reconstructed TimePix track 10 cm from the SIPM for the 6-layer module.

Table A.9: The single hit efficiency for a given seed, neighbour and sum threshold for the respective DUT at the mirror (A) and near the SIPM (C) for different angles. The text in bold is the foreseen thresholds for the LHCb Upgrade.

Seed	Neighbour	Sum	(A) 0°	(A) 10°	(C) 0°	(C) 10°
			6-layer module			
1.5	0.5	1.5	0.9989 ± 0.0003	0.9991 ± 0.0002	0.9985 ± 0.0003	0.9997 ± 0.0002
1.5	1.5	1.5	0.9989 ± 0.0003	0.9991 ± 0.0002	0.9984 ± 0.0004	0.9997 ± 0.0002
2.0	1.5	1.5	0.9964 ± 0.0004	0.9958 ± 0.0004	0.9983 ± 0.0004	0.9996 ± 0.0002
2.5	1.5	1.5	0.9928 ± 0.0007	0.9926 ± 0.0005	0.9983 ± 0.0004	0.9995 ± 0.0002
3.0	1.5	1.5	0.9859 ± 0.0009	0.9808 ± 0.0007	0.9979 ± 0.0004	0.9993 ± 0.0002
3.5	1.5	1.5	0.9759 ± 0.0011	0.9703 ± 0.0009	0.9973 ± 0.0005	0.9986 ± 0.0003
4.0	1.5	1.5	0.9593 ± 0.0014	0.9464 ± 0.0011	0.9961 ± 0.0005	0.9968 ± 0.0003
4.5	1.5	1.5	0.9375 ± 0.0018	0.9204 ± 0.0014	0.9948 ± 0.0007	0.9943 ± 0.0004
2.5	**1.5**	**4.5**	0.9803 ± 0.0011	0.9782 ± 0.0008	0.9974 ± 0.0004	0.9992 ± 0.0002
			8-layer module			
1.5	0.5	1.5	0.9987 ± 0.0002	0.9988 ± 0.0003	0.9982 ± 0.0003	0.9994 ± 0.0002
1.5	1.5	1.5	0.9986 ± 0.0002	0.9988 ± 0.0003	0.9981 ± 0.0002	0.9995 ± 0.0002
2.0	1.5	1.5	0.9961 ± 0.0003	0.9959 ± 0.0004	0.9980 ± 0.0002	0.9994 ± 0.0002
2.5	1.5	1.5	0.9933 ± 0.0004	0.9922 ± 0.0006	0.9979 ± 0.0003	0.9994 ± 0.0002
3.0	1.5	1.5	0.9847 ± 0.0005	0.9815 ± 0.0008	0.9973 ± 0.0003	0.9985 ± 0.0003
3.5	1.5	1.5	0.9752 ± 0.0007	0.9671 ± 0.0011	0.9968 ± 0.0003	0.9968 ± 0.0005
4.0	1.5	1.5	0.9551 ± 0.0009	0.9404 ± 0.0014	0.9948 ± 0.0004	0.9936 ± 0.0006
4.5	1.5	1.5	0.9350 ± 0.0010	0.9058 ± 0.0018	0.9927 ± 0.0004	0.9876 ± 0.0008
2.5	**1.5**	**4.5**	0.9824 ± 0.0006	0.9794 ± 0.0009	0.9975 ± 0.0003	0.9985 ± 0.0003

Table A.10: The single hit efficiency for a given seed, neighbour and sum threshold for the 6-layer module at the mirror (A). The text in bold is the foreseen thresholds for the LHCb Upgrade.

Seed	Neighbour	Sum	Hit Eff.
1.5	0.5	1.5	0.9989 ± 0.0003
1.5	1.5	1.5	0.9989 ± 0.0003
2.0	1.5	1.5	0.9964 ± 0.0004
2.5	1.5	1.5	0.9928 ± 0.0007
3.0	1.5	1.5	0.9859 ± 0.0009
3.5	1.5	1.5	0.9759 ± 0.0011
4.0	1.5	1.5	0.9593 ± 0.0014
4.5	1.5	1.5	0.9375 ± 0.0018
2.5	**1.5**	**4.5**	0.9803 ± 0.0011

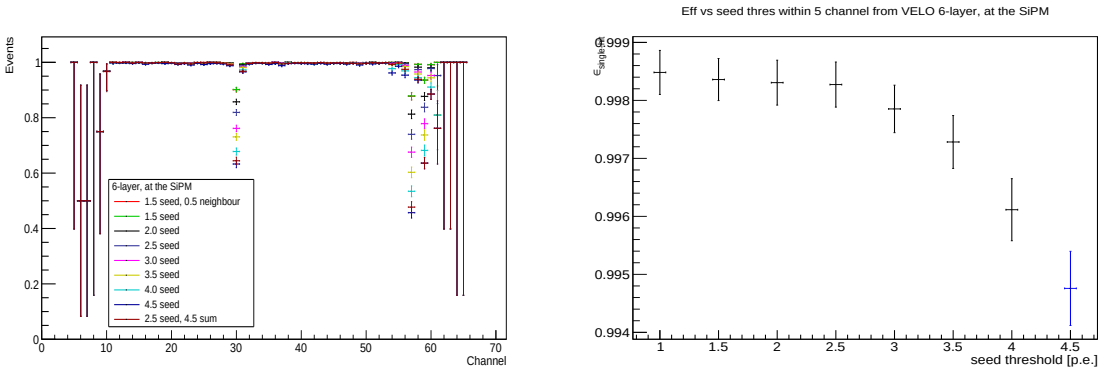

Figure A.13: Single-hit efficiency vs. SiPM channels ID (left) 10cm from the SiPM. On the right, the efficiency at the plateau for channels away from the gap is plotted against the seed threshold. Both plots correspond to the 6-layer module.

Table A.11: The single hit efficiency for a given seed, neighbour and sum threshold for the 6-layer module 10 cm from the SiPM (C). The text in bold is the foreseen thresholds for the LHCb Upgrade.

Seed	Neighbour	Sum	Hit Eff.
1.5	0.5	1.5	0.9985 ± 0.0003
1.5	1.5	1.5	0.9984 ± 0.0004
2.0	1.5	1.5	0.9983 ± 0.0004
2.5	1.5	1.5	0.9983 ± 0.0004
3.0	1.5	1.5	0.9979 ± 0.0004
3.5	1.5	1.5	0.9973 ± 0.0005
4.0	1.5	1.5	0.9961 ± 0.0005
4.5	1.5	1.5	0.9948 ± 0.0007
2.5	**1.5**	**4.5**	0.9974 ± 0.0004

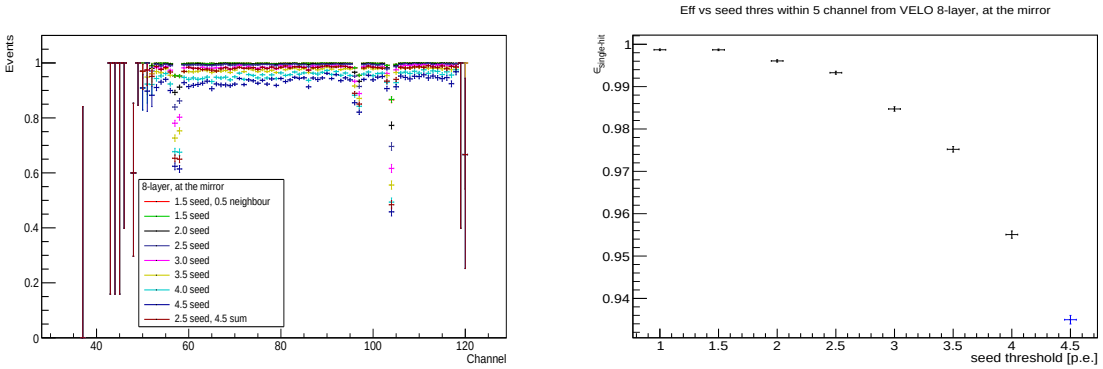

Figure A.14: Single-hit efficiency vs. SiPM channels ID (left) at the mirror. On the right, the efficiency at the plateau for channels away from the gap is plotted against the seed threshold. Both plots correspond to the 8-layer module.

Table A.12: The single hit efficiency for a given seed, neighbour and sum threshold for the 8-layer module at the mirror (A). The text in bold is the foreseen thresholds for the LHCb Upgrade.

Seed	Neighbour	Sum	Hit Eff.
1.5	0.5	1.5	0.9987 ± 0.0002
1.5	1.5	1.5	0.9986 ± 0.0002
2.0	1.5	1.5	0.9961 ± 0.0003
2.5	1.5	1.5	0.9933 ± 0.0004
3.0	1.5	1.5	0.9847 ± 0.0005
3.5	1.5	1.5	0.9752 ± 0.0007
4.0	1.5	1.5	0.9551 ± 0.0009
4.5	1.5	1.5	0.9350 ± 0.0010
2.5	**1.5**	**4.5**	0.9824 ± 0.0006

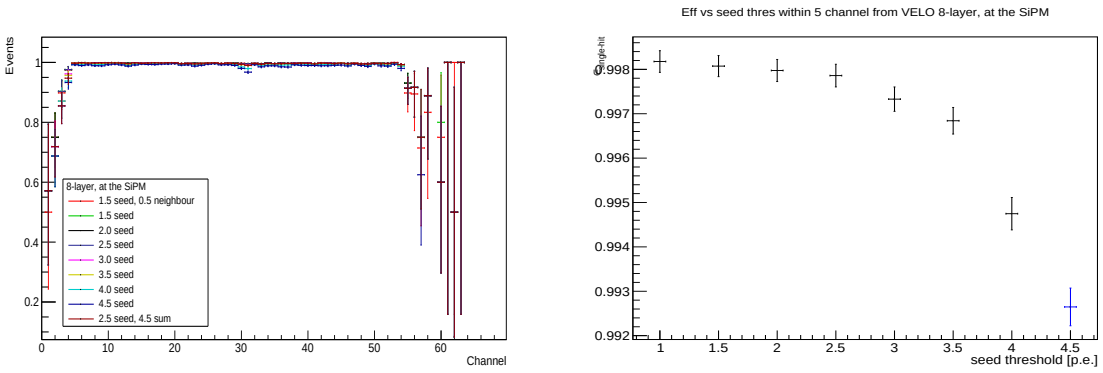

Figure A.15: Single-hit efficiency vs. SiPM channels ID (left) 10cm from the SiPM. On the right, the efficiency at the plateau for channels away from the gap is plotted against the seed threshold. Both plots correspond to the 8-layer module.

Table A.13: The single hit efficiency for a given seed, neighbour and sum threshold for the 8-layer module 10 cm from the SiPM (C). The text in bold is the foreseen thresholds for the LHCb Upgrade.

Seed	Neighbour	Sum	Hit Eff.
1.5	0.5	1.5	0.9982 ± 0.0003
1.5	1.5	1.5	0.9981 ± 0.0002
2.0	1.5	1.5	0.9980 ± 0.0002
2.5	1.5	1.5	0.9979 ± 0.0003
3.0	1.5	1.5	0.9973 ± 0.0003
3.5	1.5	1.5	0.9968 ± 0.0003
4.0	1.5	1.5	0.9948 ± 0.0004
4.5	1.5	1.5	0.9927 ± 0.0004
2.5	**1.5**	**4.5**	0.9975 ± 0.0003

References

[1] LHCb collaboration, R. Aaij *et al.*, *Framework TDR for the LHCb Upgrade*, Apr, 2012.

[2] LHCb collaboration, *LHCb Tracker Upgrade Technical Design Report*, CERN-LHCC-2014-001. LHCb-TDR-015.

[3] C. Joram *et al.*, *LHCb Scintillating Fibre Tracker Engineering Design Review Report: Fibres, Mats and Modules*, Tech. Rep. LHCb-PUB-2015-008. CERN-LHCb-PUB-2015-008, CERN, Geneva, Mar, 2015.

[4] R. Greim *et al.*, *A New Measurement of the Cosmic-Ray Flux Below 5GV Rigidity with the PERDaix Detector*, in *Proceedings of the 20th ESA Symposium on European Rocket and Balloon Programmes and Related Research*, (Hyère, France), 2011.

[5] C. Joram and T. Schneider, *Mirroring of fibre ends for the LHCb SciFi project*, Tech. Rep. LHCb-PUB-2014-020. CERN-LHCb-PUB-2014-020. LHCb-INT-2013-060, CERN, Geneva, Feb, 2014.

[6] C. Joram *et al.*, *Irradiation test of mirror samples for the LHCb SciFi tracker*, Tech. Rep. LHCb-PUB-2016-006. CERN-LHCb-PUB-2016-006, CERN, Geneva, Feb, 2016.

[7] S. Callier, C. D. Taille, G. Martin-Chassard, and L. Raux, *EASIROC, an Easy & Versatile ReadOut Device for SiPM*, Phys. Procedia **37** (2012) 1569.

[8] B. Beischer *et al.*, *A High-resolution Scintillating Fiber Tracker With Silicon Photomultiplier Array Readout*, Nucl. Instrum. Meth. **A622** (2010) 542.

[9] C. Joram and U. Uwer, *LHCb Scintillating Fibre Tracker Engineering Design Review: Frontend Electronics*, Tech. Rep. LHCb-PUB-2016-012. CERN-LHCb-PUB-2016-012, CERN, Geneva, Jun, 2016.

[10] P. Azzarello, *Tests and production of the AMS-02 silicon tracker detectors*, PhD thesis, Université de Genève, 2004.

[11] LHCb, *The Timepix Telescope for High Performance Particle Tracking*, .

[12] B. Beischer *et al.*, *A high-resolution scintillating fiber tracker with silicon photomultiplier array readout*, Nucl. Instrum. Meth. **A622** (2010) 542, `arXiv:1011.0226`.

[13] A. Fasso *et al.*, *FLUKA: a multi-particle transport code*, 2005. CERN-2005-10, INFN/TC05/11, SLAC-R-773.

[14] G. Battistoni *et al.*, *The FLUKA code: Description and benchmarking*, in *Proceedings of the Hadronic Shower Simulation Workshop 2006* (M. Albrow and R. Raja, eds.), AIP Conference Proceeding 896, pp. 31–49, 2007.

[15] F. Ravotti *et al.*, *A New High-Intensity Proton Irradiation Facility at the CERN PS East Area*, in *Proc. Technology and Instrumentation in Particle Physics Conference TIPP 2014*, Amsterdam, the Netherlands, 2-6 June 2014. PoS(TIPP2014)354.

[16] A. B. Rodrigues Cavalcante *et al.*, *Irradiation of a 2.5 m long SciFi module with 24 GeV/c protons to the dose profile expected in LHCb*, Tech. Rep. LHCb-PUB-2016-001. CERN-LHCb-PUB-2016-001, CERN, Geneva, Jan, 2016.

[17] B. Leverington, C. Joram, and S. Baker, *Scintillating Fibre Irradiation with 22.9 MeV Protons*, Tech. Rep. LHCb-PUB-2014-024, CERN-LHCb-PUB-2014-024, LHCb-INT-2014-002, CERN, Geneva, Jan, 2014.

[18] M. Deckenhoff and B. Spaan, *Scintillating Fibre and Silicon Photomultiplier Studies for the LHCb upgrade*, PhD thesis, Dortmund U., Dec, 2015, Presented 23 Feb 2016.

[19] R. J. Ekelhof and B. Spaan, *Studies for the LHCb SciFi Tracker - Development of Modules from Scintillating Fibres and Tests of their Radiation Hardness*, PhD thesis, Dortmund, Technische Universität Dortmund, Mar, 2016, Presented 18 May 2016.